CHALMERS

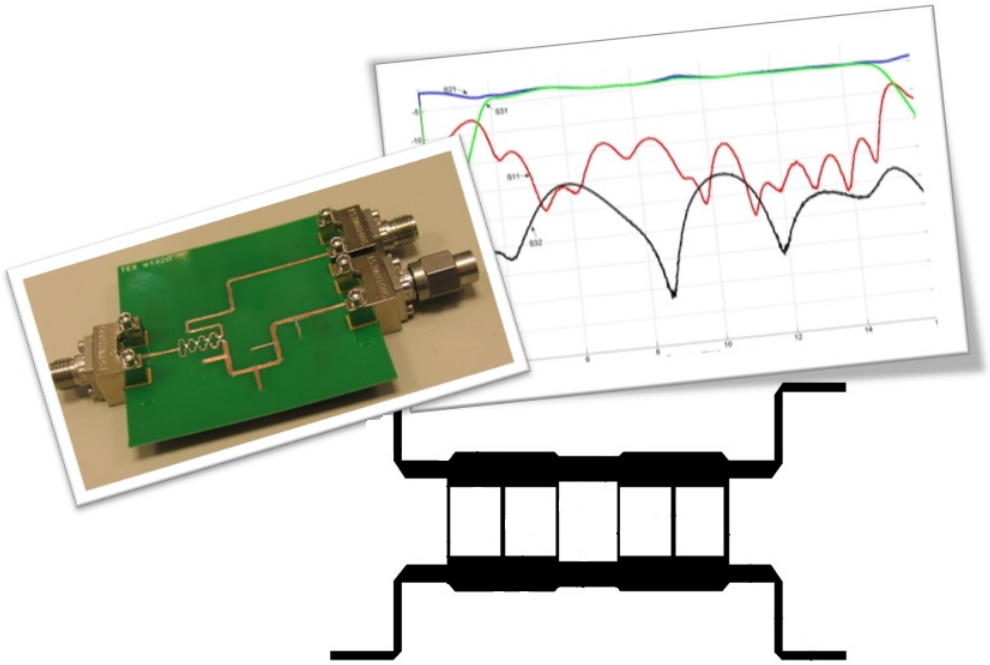

Wideband Directional Couplers and Power Splitters

Thesis for the degree of Master of Science

ELMIN TUTKUR

Department of Earth & Space Sciences
Chalmers University of Technology
Gothenburg, Sweden
Master's Thesis 2014

Wideband Directional Couplers and Power Splitters

A thesis submitted in partial fulfilment of the requirements for the degree of Master of Science

ELMIN TUTKUR

Department of Earth & Space Sciences
CHALMERS UNIVERSITY OF TECHNOLOGY
Gothenburg, Sweden, 2014

Wideband Directional Couplers and Power Splitters
ELMIN TUTKUR

Thesiswork completed at:
Division of Microwaves and Antennas
SAAB Electronic Defence Systems
SE431 45 Molndal, Sweden

Supervisor and examiner:
Assoc. Prof. Vincent Desmaris
Department of Earth & Space Sciences
Chalmers University of Technology
vincent.desmaris@chalmers.se

Supervisors:
Wolfgang Staberg
Division of Microwaves and Antennas
SAAB Electronic Defences Systems
wolfgang.staberg@saabgroup.com

Prof. Hans-Olof Vickes
Division of Microwaves and Antennas
SAAB Electronic Defence Systems
hans-olof.vickes@saabgroup.com

Cover picture: Photograph of the suggested wideband 180° power splitter, the S-parameter characteristics of the photographed power splitter and microstrip layout for a suggested quadrature hybrid.

Chalmers University of Technology
Department of Earth & Space Sciences
Gothenburg, Sweden, June 2014

Abstract

Microwave quadrature couplers and out-of-phase power combiners/dividers are in many aspects crucial devices and are used in many microwave subsystems, such as mixers, modulators, antenna beam forming networks and antenna array feeds to name a few. In modern microwave circuits there is an increasing demand for wideband operation and lower costs (no complex structures), and thus the power couplers/dividers must follow the same requirements. This thesis presents the design and characterisation of four different quadrature hybrid designs based on a Branch Line Coupler (BLC) core structure and a 180° power splitter through a combination of a wideband Wilkinson power divider and a phase shifting network at the output ports. The manufactured quadrature hybrid measured a 60 % fractional bandwidth (6.5 GHz - 12 GHz) with a maximum amplitude and phase imbalance of 0.5 dB and ±5.8° respectively. Return loss better than 11 dB and isolation better than 15 dB was achieved over the whole operational bandwidth. Regarding the out-of-phase power divider a 110% fractional bandwidth (4.31 GHz - 14.97 GHz) was achieved with return loss and isolation better than 13.5 dB and 20 dB respectively, accompanied by an amplitude and phase imbalance of 0.5 dB and ±13.4°. All proposed circuits were constructed on a single commercially available dielectric substrate in a microstrip structure.

Keywords: Quadrature Coupler, Wideband, BLC (Branch Line Coupler), Power Splitter, Phase shifter, 180 degree power splitter, Fabrication

Acknowledgements

First of all I would like to thank the people at SAAB EDS for providing me with the opportunity to carry out this thesis at their facilities in Molndal. I would like to give a special acknowledgement to Ingvar Sundvall and my supervisors prof. Hans-Olof Vickes and Wolfgang Staberg for their guidance throughout this whole project.

Furthermore I would like to thank my examiner from Chalmers, Assoc. Prof. Vincent Desmaris for taking on this project with me and and going beyond the requirements put on him to aid me in this thesis work. Finally I want to give a special thanks to Hawal Rashid, ph.D. student at Chalmers, for valuable discussions and insight.

Elmin Tutkur, Gothenburg 06/2014

Contents

1

Introduction

The ability to distribute and combine signals is a very fundamental and important function in many microwave systems, this is particularly useful if it can be done over a wide frequency range and with phase shifted signals. Power dividers and directional couplers, are indispensable passive components used in several microwave systems, i.e., mixers, modulators and antenna beam-forming networks. One of the drawbacks with directional couplers is the inherited poor bandwidth due to the fact that best coupling is achieved when the electrical length of the transmission line is a quarter wavelength of the center frequency. The most common solution to the narrow bandwidth problem is to cascade several sections together, the trade-off is larger geometries together with poor directivity, increased losses and coupling errors due to discontinuities in line widths.

1.1 Background

Future multifunctional radar systems require large bandwidths (several octaves), inherent in such systems are functional blocks, i.e. 180° hybrids and Branch Line Couplers (BLC). Furthermore the 180° hybrids are important as basic circuits in balanced mixers, antenna feed networks and push-pull amplifiers or at any other place where there is a need for conversion between balanced and unbalanced signals. An important aspect and a great challenge is also to realise the circuits on existing Printed Circuit Board (PCB) materials for easy manufacturing (standard commercial processes) and integration.

1.2 Objective

The objective of this thesis is to design and evaluate two types of directional couplers for wideband operation: a quadrature (90°) hybrid and a 180° hybrid. The capabilities and limitations of specific coupler designs should be studied. The goal is to present

working prototypes optimised for wideband operation with the following specifications: $\pm 5^\circ$ phase-imbalance, ± 0.5 dB amplitude imbalance and better than 10 dB return loss and isolation. Geometrical limitations are not specified but should not exceed reasonable limits.

1.3 Problem Definition

The problem definition can be summarized with the following set of questions:

- How large bandwidth can be achieved utilising multi-section branch line couplers that are fabricated using low cost commercial fabrication methods and substrates?
- Are there techniques other than cascading more sections available to increase bandwidth for branch line couplers?
- Can a multi-section Wilkinson power divider combined with a phase shifting network be used to create an Ultra Wideband (UWB) 180° hybrid that can be fabricated by commercial low cost fabrication methods?

1.4 Limitations

There are a vast number of ways to realise directional couplers, and it is not within the scope of the thesis to account for them all. Specific designs have been chosen and only those will be evaluated. Designs will be limited to planar, easy to fabricate/integrate, transmission line solutions, e.g., microstrip or stripline. In other words, commercial low cost fabrication methods. These conditions come from the fact that this is a thesis done in cooperation with industry and hence the importance of cheap and robust solutions that can be mass produced. Concerning target bandwidth the objective is to explore the maximum achievable bandwidth given the pre-decided conditions regarding, phase- and amplitude-imbalance, return loss, isolation and size. With this said, the predetermined conditions are not set in stone so to say, and the interest is more towards a concept of how to realise these structures, to explore what bandwidth can be achieved and to see which parameters are the limiting ones. So some leniency towards some of the conditions for the structures can be expected.

2

Theory

This chapter will go through theory associated with power splitters and directional couplers, often referred as couplers only, beginning a brief overview of directional couplers and then different types of transmission line directional couplers will be presented. Afterwards power dividers will be treated briefly together with phase shifters and a specific broadband matching technique utilised in this work. Finally, wrapping up the theory part of this thesis there will be a section describing the fabrication method used.

2.1 Directional Couplers

Directional couplers are four-port networks which are ideally perfectly matched, lossless, reciprocal and provide a 90° or 180° phase shift between the output ports. As can be seen in figure 2.1, power is applied to port one and is coupled to port three with the coupling factor β^2. At port two, the power applied to port one is outputted, with the coefficient $\alpha^2 = 1 - \beta^2$. Ideally no power will be delivered to the isolated port, port four. However any of the ports can be defined as the input port and thus switching the through, coupled and isolation ports appropriately.

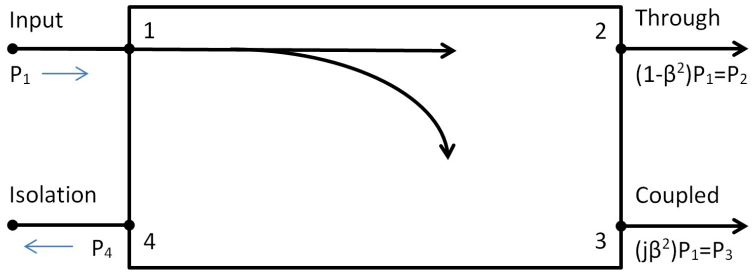

Figure 2.1: Block diagram representation of a directional coupler.

There are certain quantities used to define the characteristics of the directional coupler:

$$Coupling = C = 10\log\frac{P_1}{P_3} = -20\log\beta\ dB \tag{2.1a}$$

$$Directivity = D = 10\log\frac{P_3}{P_4} = 20\log\frac{\beta}{|S_{14}|}\ dB \tag{2.1b}$$

$$Isolation = I\ = 10\log\frac{P_1}{P_4} = -20\log|S_{14}|\ dB \tag{2.1c}$$

$$Insertion\ Loss = L = 10\log\frac{P_1}{P_2} = -20\log|S_{12}|\ dB \tag{2.1d}$$

The *coupling* indicates the fraction of input power that is coupled to port three. The *directivity* says how well the coupler manages to isolate forward and backward waves. The *isolation* provides the fraction of power delivered to the uncoupled/isolated port. And finally the *insertion loss* account for the amount of power delivered to the through port, diminished by power delivered to the coupled and isolated ports. In an ideal coupler the directivity and isolation are infinite [1].

Directional couplers can be divided in two subgroups of couplers, the 90° (quadrature) couplers and the 180° couplers. There are special cases of directional couplers called *hybrid couplers* or *3 dB hybrids* which implies an even power distribution between the coupled and the through port ($\beta = \frac{1}{\sqrt{2}}$). The quality of these devices is determined by the amplitude and phase imbalances, meaning the difference in amplitude between the two output ports and how much the phase differs from the desired 90° or 180° between the two output ports. The succeeding sections will describe the most common realisations of quadrature and 180° hybrids. Even though many of the designs can be applied to waveguide techniques as well, this section will almost exclusively focus on the transmission line realisations.

2.1.1 Branch Line Coupler

The first example of a quadrature coupler is the branch line coupler illustrated in figure 2.2. The figure illustrates a branch line hybrid, but uneven power split between the two output ports at the center frequency can be achieved by changing the characteristic impedance of the transmission lines between the ports. Observing figure 2.2 the basic operation of a branch line hybrid is as follows. Assuming that all ports are matched, the power applied at port one is evenly divided between ports two and three with a 90° phase difference between the two outputs. No power is coupled to the isolated port, port 4 [1]. The branch line hybrid is very attractive for implementation due to the advantages of having an entirely planar structure together with a simple and robust design.

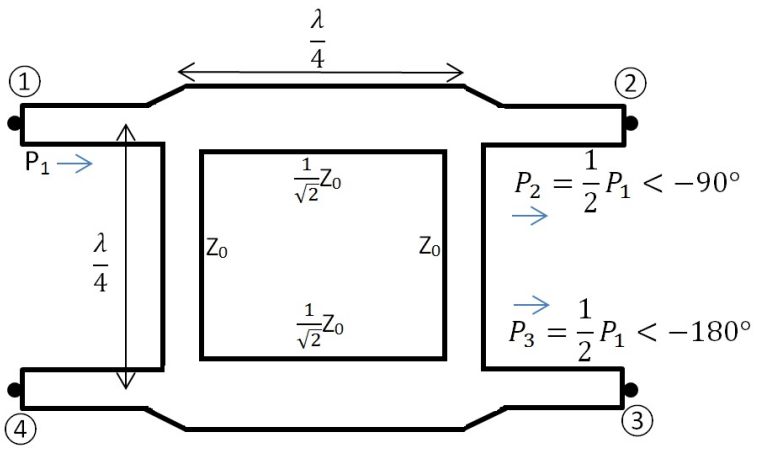

Figure 2.2: An ideal branch line hybrid.

The bandwidth of a single stage branch line coupler is, as for other couplers, limited by its electrical length, in this case a quarter wavelength. A single branch line coupler section is therefore not very suitable for wideband operation, having a limited bandwidth of $10\% - 20\%$ [2]. Though adding more sections in a cascade can increase the bandwidth to almost one octave [3] it comes with a price of increasing chip size and complicating the fabrication process due to transmission line impedances becoming very impractical. For conventional microstrip designs the limit is around 4 branches, more sections than this and the outer branch impedances are too high to be fabricated.

A method of analysis for the four port symmetrical network, such as a branch line coupler, is even and odd mode analysis. The method makes it possible to determine the resultant signals appearing at the four ports and how they vary in phase and amplitude, depending on frequency [4].

A schematic circuit of the branch line coupler normalised with respect to the characteristic admittance Y_0 can be observed in figure 2.3. Decomposing this network into

an even- and odd-mode excitation as in figure 2.4, the four-port is reduced into a pair of two-port networks. Looking at the incident signals in figure 2.4a and since the opposing signal (at port four) has the same magnitude and phase as the one at port one, it will appear as if the signal from port one was perfectly reflected at the line of symmetry, resulting in the open circuited stubs. Similarly and with the same reasoning as for the even mode circuit but with a reflection coefficient of -1, the short-circuited stubs in figure 2.4b can be explained. One can also see it as voltage maximums/minimums appearing one line of symmetry/anti-symmetry for the even- and odd-mode respectively.

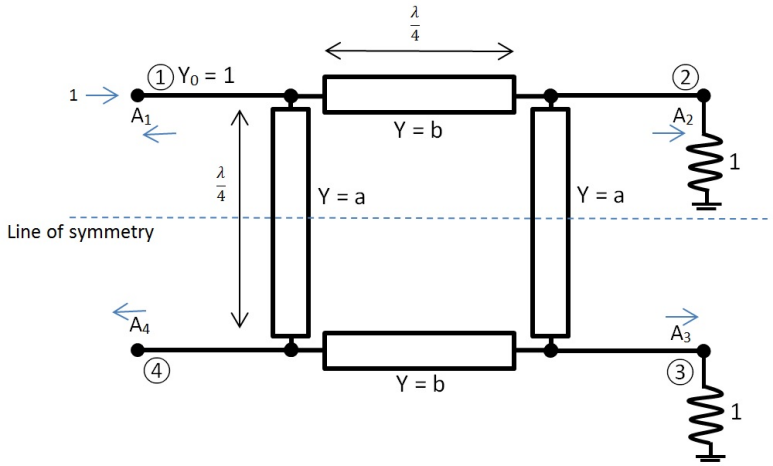

Figure 2.3: Schematic circuit of the branch line coupler in normalized form.

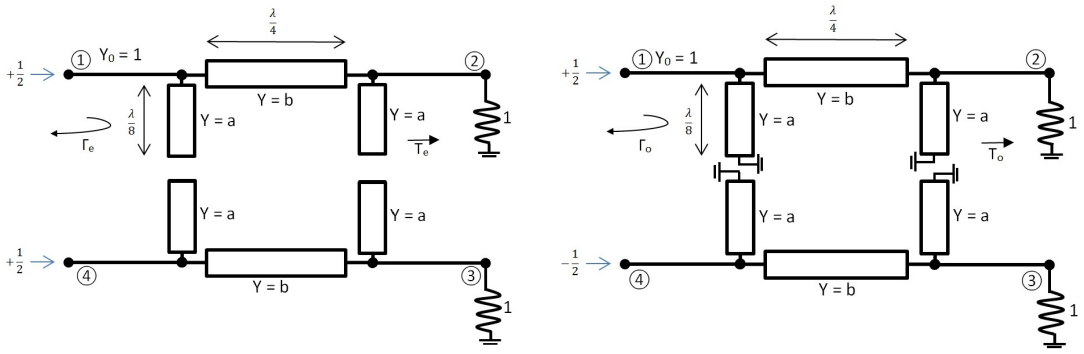

Figure 2.4: The resulting equivalent decomposition of a branch line coupler into even- and odd-mode excitations. (a) Even-mode excitation (e). (b) Odd-mode excitation (o).

By superposition, the sum of the two-port solutions provides the resultant signals out of the four ports in figure 2.3 [4]. The amplitude of the incident signal of the four-port

in figure 2.3 is assumed to be of unit amplitude, resulting in amplitudes of $\pm\frac{1}{2}$ in the even- and odd-mode circuits. The emerging signal at each port of the branch line hybrid can then be expressed as:

$$A_1 = \frac{1}{2}\Gamma_e + \frac{1}{2}\Gamma_o \tag{2.2a}$$

$$A_2 = \frac{1}{2}T_e + \frac{1}{2}T_o \tag{2.2b}$$

$$A_3 = \frac{1}{2}T_e - \frac{1}{2}T_o \tag{2.2c}$$

$$A_4 = \frac{1}{2}\Gamma_e - \frac{1}{2}\Gamma_o \tag{2.2d}$$

where $\Gamma_{e,o}$ and $T_{e,o}$ are the even- and odd-mode reflection and transmission coefficients as in figure 2.4. The calculation of the reflection and transmission coefficient can be done by multiplying the ABCD matrices of each cascade component in that circuit. The ABCD parameters can then be converted to S parameters which are equivalent to the reflection and transmission coefficients (assuming that all ports are matched) [1, 4]:

$$\Gamma = \frac{A + B - C - D}{A + B + C + D} \tag{2.3a}$$

$$T = \frac{2}{A + B + C + D} \tag{2.3b}$$

The individual matrices for each component can easily be found in table 4.1 of [1]. The resulting ABCD matrix for the even-mode excitation, assuming lossless lines and admittances according to figure 2.4a:

$$\begin{bmatrix} A & B \\ C & D \end{bmatrix}_e = \begin{bmatrix} 1 & 0 \\ ja & 1 \end{bmatrix} \begin{bmatrix} 0 & \frac{j}{b} \\ jb & 0 \end{bmatrix} \begin{bmatrix} 1 & 0 \\ ja & 1 \end{bmatrix} = \begin{bmatrix} -\frac{a}{b} & \frac{j}{b} \\ j(b - \frac{a^2}{b}) & -\frac{a}{b} \end{bmatrix} \tag{2.4}$$

Applying the same procedure to the odd-mode excitation, admittances according to figure 2.4b:

$$\begin{bmatrix} A & B \\ C & D \end{bmatrix}_o = \begin{bmatrix} 1 & 0 \\ -ja & 1 \end{bmatrix} \begin{bmatrix} 0 & \frac{j}{b} \\ jb & 0 \end{bmatrix} \begin{bmatrix} 1 & 0 \\ -ja & 1 \end{bmatrix} = \begin{bmatrix} \frac{a}{b} & \frac{j}{b} \\ j(b - \frac{a^2}{b}) & \frac{a}{b} \end{bmatrix} \tag{2.5}$$

As expected the requirement for forward-to-back symmetry (A=D) is fulfilled in both cases. Using equation 2.3a and 2.3b the reflection and transmission coefficients for the

two modes are extracted:

$$\Gamma_e = \frac{-\frac{a}{b} + \frac{j}{b} - j(b - \frac{a^2}{b}) + \frac{a}{b}}{-\frac{a}{b} + \frac{j}{b} + j(b - \frac{a^2}{b}) - \frac{a}{b}} \tag{2.6a}$$

$$T_e = \frac{2}{-\frac{a}{b} + \frac{j}{b} + j(b - \frac{a^2}{b}) - \frac{a}{b}} \tag{2.6b}$$

$$\Gamma_o = \frac{\frac{a}{b} + \frac{j}{b} - j(b - \frac{a^2}{b}) - \frac{a}{b}}{\frac{a}{b} + \frac{j}{b} + j(b - \frac{a^2}{b}) + \frac{a}{b}} \tag{2.6c}$$

$$T_o = \frac{2}{\frac{a}{b} + \frac{j}{b} + j(b - \frac{a^2}{b}) + \frac{a}{b}} \tag{2.6d}$$

Since the device is symmetric ($A = D$) and the condition for reciprocity is $AB = CD$ it implies that $B = C$. Also looking at the reflection coefficients Γ_e and Γ_o, if the device is to be perfectly matched and directive they need to be set to zero, in other words, $B = C$ in both the even and the odd matrices, which gives us the following relation: $a^2 = b^2 - 1$. Utilising equations 2.2a-2.2d:

$$A_1 = 0 \tag{2.7a}$$

$$A_2 = -\frac{j}{b} \tag{2.7b}$$

$$A_3 = \frac{\sqrt{b^2 - 1}}{b} \tag{2.7c}$$

$$A_4 = 0 \tag{2.7d}$$

To achieve even power split between ports two and three and setting $a = 1$ one gets that $b = \sqrt{2}$, switching to impedance values instead it means that if the branch impedance is Z_0 then the line impedance needs to be $\frac{Z_0}{\sqrt{2}}$ for equal power split. The method described, *odd- and even-mode analysis*, can be used to analyse more complex designs with multiple sections, matching stubs and so on, it simply just means adding more component matrices. The algebraic expressions in the ABCD-matrices easily get out of hand when cascading several sections together to form a multi-section branch line coupler. Help functions can be introduced to simplify the problem and then mathematical software is used to solve the resulting equation systems numerically [5, 6].

If one wants to calculate the frequency sensitivity then the frequency dependent values in the matrices can be expressed in terms of $t = \tan(\frac{\pi l}{\lambda})$. In the case of the branch line hybrid as before, the resulting ABCD-matrices would be of the form:

$$\begin{bmatrix} A & B \\ C & D \end{bmatrix}_e = \begin{bmatrix} 1 & 0 \\ jat & 1 \end{bmatrix} \begin{bmatrix} \frac{1-t^2}{1+t^2} & \frac{j2t}{b(1+t^2)} \\ \frac{jb2t}{1+t^2} & \frac{1-t^2}{1+t^2} \end{bmatrix} \begin{bmatrix} 1 & 0 \\ jat & 1 \end{bmatrix} \tag{2.8}$$

$$\begin{bmatrix} A & B \\ C & D \end{bmatrix}_o = \begin{bmatrix} 1 & 0 \\ \frac{-ja}{t} & 1 \end{bmatrix} \begin{bmatrix} \frac{1-t^2}{1+t^2} & \frac{j2t}{b(1+t^2)} \\ \frac{jb2t}{1+t^2} & \frac{1-t^2}{1+t^2} \end{bmatrix} \begin{bmatrix} 1 & 0 \\ \frac{-ja}{t} & 1 \end{bmatrix} \tag{2.9}$$

Note that:

$$\cos(\frac{2\pi l}{\lambda}) = \frac{1 - \tan^2(\frac{\pi l}{\lambda})}{1 + \tan^2(\frac{\pi l}{\lambda})} \tag{2.10a}$$

$$\sin(\frac{2\pi l}{\lambda}) = \frac{2\tan(\frac{\pi l}{\lambda})}{1 + \tan^2(\frac{\pi l}{\lambda})} \tag{2.10b}$$

As an example one could take the values of a and b calculated above for a 3 dB hybrid and enter those values in the ABCD matrices to plot the frequency dependence of the signals at the four ports. Using scattering parameters:

$$A_1 = S_{11} \tag{2.11a}$$

$$A_2 = S_{21} \tag{2.11b}$$

$$A_3 = S_{31} \tag{2.11c}$$

$$A_4 = S_{41} \tag{2.11d}$$

The resulting graph can be seen in figure 2.5:

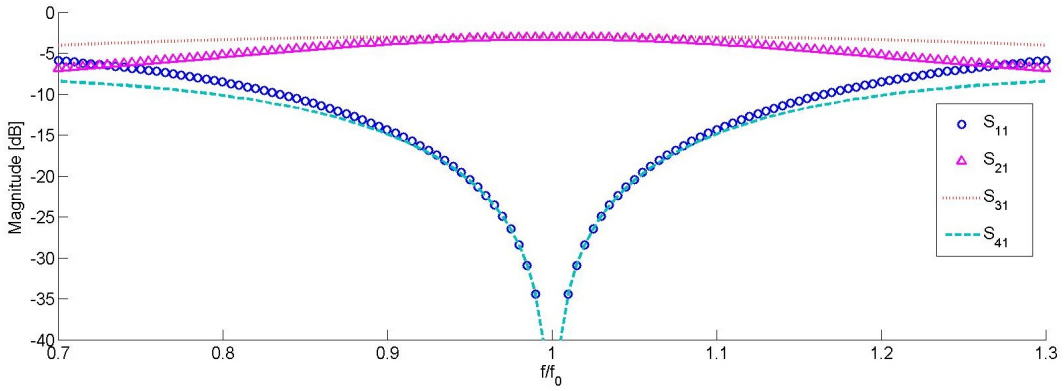

Figure 2.5: A plot illustrating frequency characteristics of an ideal branch line hybrid calculated using even- and odd-mode analysis described above. The frequency is normalised with respect to the design frequency f_0

2.1.2 Coupled Line Coupler

If one brings two unshielded transmission lines in close proximity to each other, like in figure 2.6, energy can be coupled from one line to the other due to the interaction of the electromagnetic fields. These lines are referred to as *coupled transmission lines*. To create a quadrature coupler out of this setup, you simply make the coupled section a quarter wavelength long. There are atleast three ways to couple the lines: broadside coupled, edge coupled and end coupled. In the case of a quadrature coupler, where one needs a quarter-wave section, only the first two are appropriate. A cross section representation of these two geometries can be seen in figure 2.7.

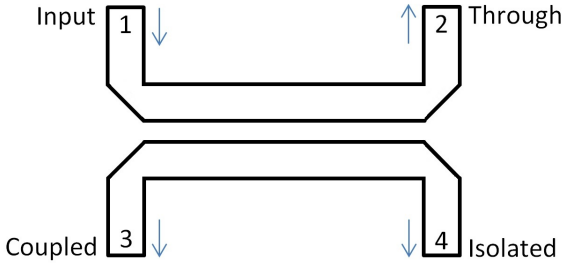

Figure 2.6: A coupled line coupler.

The bandwidth of the coupled line coupler is often better than for a direct coupler like the branch line coupler but it is also limited by the electrical length of the coupler, which is a quarter wavelength long at the center frequency. However just as for the other case one can increase the bandwidth by cascading several sections together with different degree of coupling between them (weakest coupling at the edges). But when strong coupling (higher than 6-8 dB) [7] is required, only broadside coupling (see figure 2.7b) is practical to use. This is because edge coupled transmission lines require such narrow separation that it requires resolutions higher than commercial fabrication methods can offer [8].

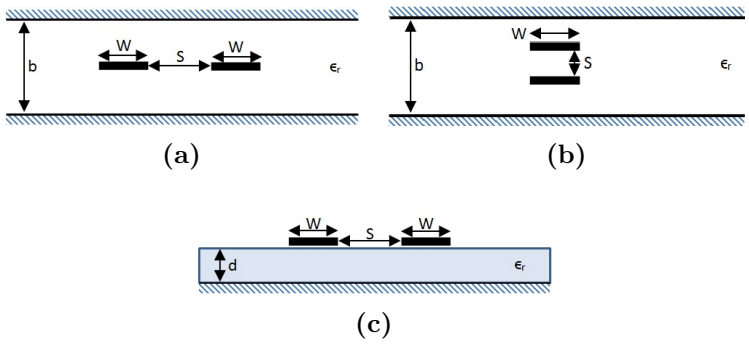

Figure 2.7: Different transmission line geometries. (a) Edge or planar coupled stripline. (b) Broadside coupled stripline. (c) Edge or planar coupled microstrip.

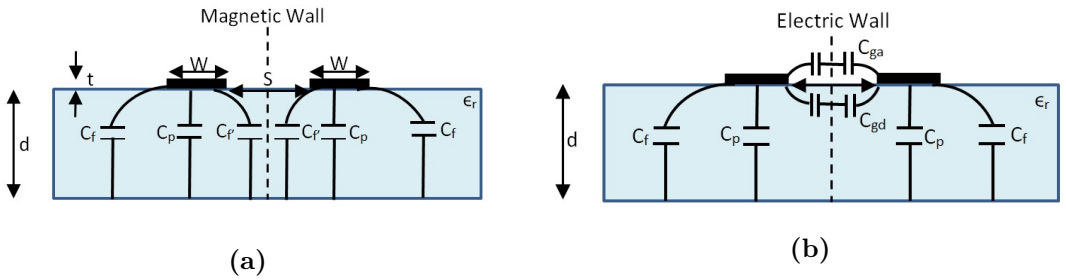

Figure 2.8: The resulting equivivalent capactiance networks for an even- and odd-mode excitation for a coupled microstrip line. (a) Even-mode excitation. (b) Odd-mode excitation.

The microstrip coupled line shown in figure 2.7c can be represented by the equivalent circuit shown in figure 2.8 [9]. Using the even- and odd-mode impedances one can determine the electrical characteristics of the coupled lines. The impedances are obtained from the total even- and odd-mode capacitance values from figure 2.8, which are as follows:

$$C_e = C_p + C_f + C_{f'} \tag{2.12a}$$
$$C_o = C_p + C_f + C_{ga} + C_{gd} \tag{2.12b}$$

Where C_p is the parallel plate capacitance ($C_p = \epsilon_0 \epsilon_r \frac{W}{d}$) and $C_f, C_{f'}, C_{ga}$ and C_{gd} are various fringing capacitances.

Using the capacitance values obtained from equation 2.12a and 2.12b one can determine the characteristic impedance as well as the effective dielectric constant for the two modes [9]:

$$Z_{0i} = c\frac{1}{\sqrt{C_i {C_i}^a}} \tag{2.13a}$$
$${\epsilon_{re}}^i = \frac{C_i}{{C_i}^a} \tag{2.13b}$$

Where i stands for even- or odd-mode, ${C_i}^a$ denotes the capacitance with air as dielectric and $c = 3 \cdot 10^8$ m/s. And finally the characteristic impedance Z_0 and the coupling coefficient β can be determined through equations 2.14a and 2.14b.

$$Z_0 = \sqrt{Z_{0e} Z_{0o}} \tag{2.14a}$$
$$\beta = \frac{Z_{0e} - Z_{0o}}{Z_{0e} + Z_{0o}} \tag{2.14b}$$

2.1.3 Lange Couplers

When coupling factors stronger than 6 dB are desired, simple coupled line couplers are not suitable. One can turn to the broadside coupler but they are difficult to implement using microstrip technology. There are some solutions to this problem and one of them is the *Lange Coupler*, see figure 2.9. By using a layout of several lines parallel to each other, one can utilize the fringing fields on both sides of the for the coupling instead of on just the one side like in standard coupled line couplers. This design can easily achieve 3 dB coupling ratios, with more than one octave bandwidth. It also tends to compensate for different even- and odd-mode phase velocities, which improves the bandwidth [1]. There are disadvantages as well, and probably the biggest one is the *interdigitated* geometry, which refers to the required bonding wires or air bridges between the lines. This together with the narrow separation of the lines can complicate the fabrication procedures. However the fact that the whole structure can be fabricated using lithographic methods makes this a very suitable option for high coupling requirements are desired in microstrip layouts.

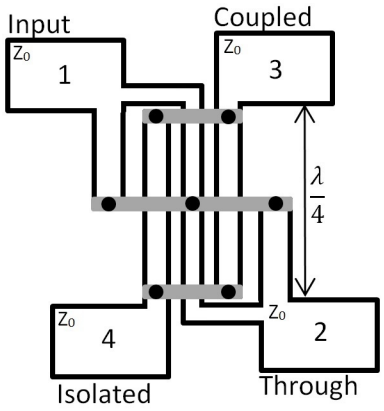

Figure 2.9: Lange coupler layout in microstrip form.

2.1.4 180 Degree Hybrids

The 180° hybrid is a similar four port network as the quadrature hybrids, but with the ability to produce two output signals with a 180° phase difference instead of a 90° phase difference. Depending on which input port the signal is applied to, the two output signals can also be in phase. Observing figure 2.10, if a signal is applied to port one it will evenly be split, in phase, between the two output ports (ports two and three). Port four is isolated. If the input signal is applied to port four, the signal would also be equally split between the two outputs but with a 180° phase difference, and here port one is isolated. When operated the other way around, as a combiner, the sum of the two inputs at port two and three would appear at port one while the difference of the two inputs would appear at port four. Therefore ports one and four are often referred to as the sum and difference ports respectively [1].

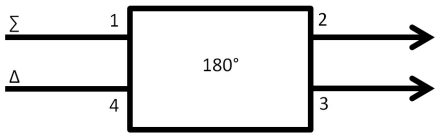

Figure 2.10: Symbol for a 180° hybrid junction.

Two common realisations of the 180° hybrid in microstrip or stripline form are the ring hybrid (or rat-race) and the tapered form, figure 2.11. The frequency dependence of the ring lengths limits the bandwidth of the ring hybrid to $20\% - 30\%$ [1]. An increase in bandwidth can be realised by adding additional sections, or with an alternate structure as in [11]. Tapered line tandem hybrids is often a wideband alternative to the rat-race coupler, but suffer from large and complex multilayer geometries [12].

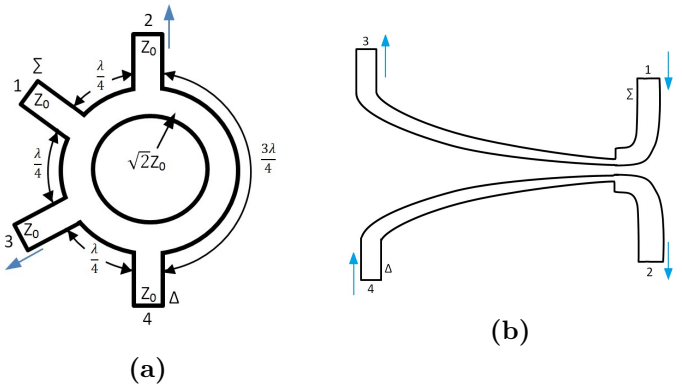

Figure 2.11: Two types of planar hybrid 180 junctions. (a) Ring hybrid or rat-race. (b) Tapered coupled line hybrid.

2.2 Wilkinson Power Divider

It can be shown that three port networks cannot be lossless, reciprocal and matched at all ports [1]. Only two conditions can be satisfied out of the three, so lossy reciprocal and matched networks are possible, a Wilkinson power divider is such a network, figure 2.12. It has the property of appearing lossless when the output ports are matched. The lossy part is the resistor between ports two and three. This solution was presented by Ernest Wilkinson in 1960, and the resistor added between the two output ports, not only allows the three ports to be matched but it fully isolates port two and three at the center frequency. The divider can be designed for arbitrary power division as or for an equal 3 dB split as in figure 2.12. It is often realised using microstrip or stripline technology. The bandwidth can be increased in the same fashion as for previous cases with couplers, by cascading several sections together [13].

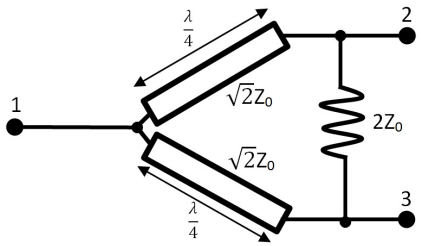

Figure 2.12: Two way split, equal amplitude, Wilkinson power divider.

The Wilkinson power divider can also be analysed by utilising the even- and odd-mode analysis as before. An equivalent transmission line circuit of the microstrip circuit in figure 2.12 can be seen in figure 2.13a. This circuit can then be redrawn so that a symmetry line appears across the midplane with all impedances normalised to the characteristic impedance Z_0, figure 2.13b. The analysis will enable the extraction of values Z and r for equal power split and scattering parameters [1]. Two modes of excitation for the circuit in figure 2.14 are defined. Even mode where $V_{g2} = V_{g3} = 2V_0$, and the odd mode where $V_{g2} = -V_{g3} = 2V_0$. Later by applying superposition of these two modes resulting in an excitation of $V_{g2} = 4V_0$ and $V_{g3} = 0$ from which the scattering parameters of the network can be extracted.

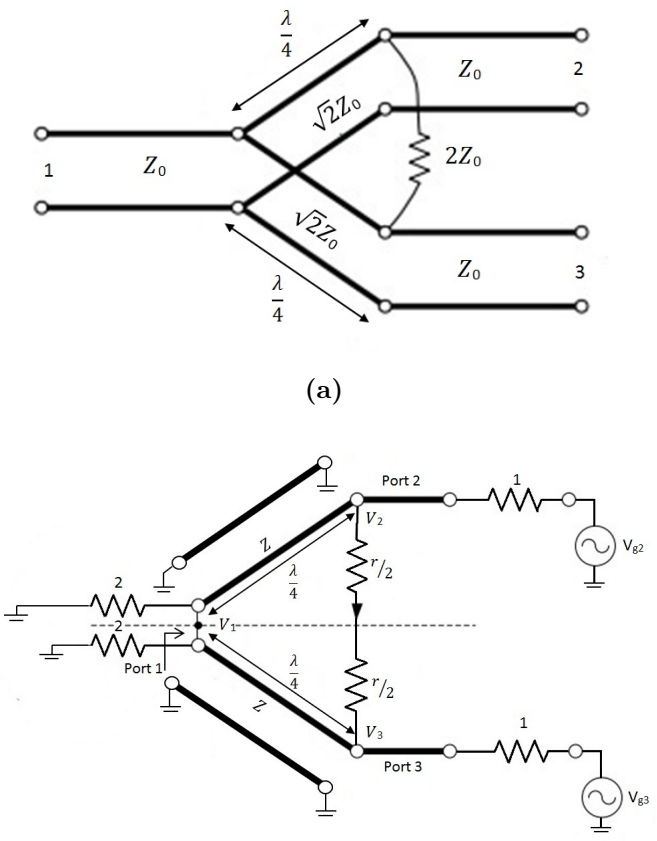

Figure 2.13: Schematic representation of the Wilkinson power divider. (a) Equivalent transmission line circuit of the microstrip circuit in figure 2.12. (b) Redrawn circuit from (a) with all impedances normalised to the characteristic impedance Z_0.

Starting with the even-mode excitation on the circuit in figure 2.13b: a symmetrical excitation as in the even-mode case causes an absence of current flow between the $\frac{r}{2}$ resistors and the short circuit between the inputs of the two transmission lines at port 1. Therefore the network can be bisected as shown in figure 2.14a to simplify the analysis.

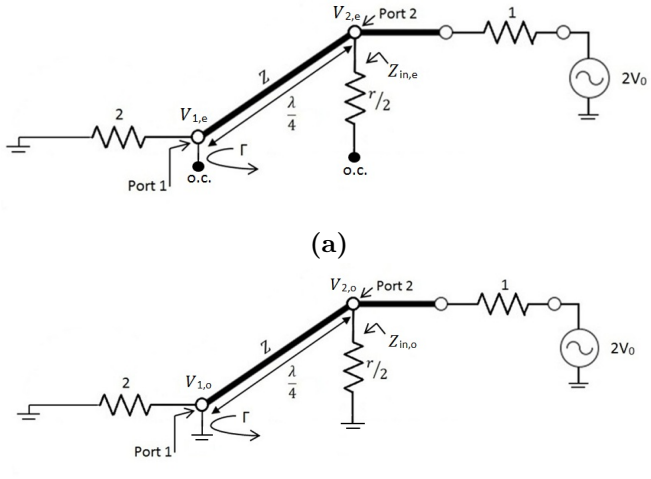

(a)

(b)

Figure 2.14: Bisected even- and odd-mode excitation circuits of the circuit in 2.13b. (a) Even-mode. (b) Odd-mode.

The circuit can be seen as a quarter wave transformer, resulting in:

$$Z_{in,e} = \frac{Z^2}{2} \tag{2.15}$$

If port two is to be matched for the even-mode excitation: $Z = \sqrt{2}$. Since $Z_{in,e} = 1$, $V_{2,e}$ can be extracted by voltage division:

$$V_{2,e} = \frac{Z_{in,e}}{Z_{in_e} + 1} V_{g2} = \frac{1}{2} 2V_0 = V_0 \tag{2.16}$$

$V_{1,e}$ can be calculated with the transmission line equation:

$$V(x) = V^+(e^{-j\beta x} + \Gamma e^{\beta x}) \tag{2.17}$$

Letting $x = 0$ at port 1 and $x = \frac{-\lambda}{4}$ at port two:

$$V_{2,e} = V(-\frac{\lambda}{4}) = V^+(e^{j\frac{2\pi\lambda}{\lambda 4}} + \Gamma e^{-j\frac{2\pi\lambda}{\lambda 4}}) = jV^+(1-\Gamma) = V_0 \tag{2.18a}$$

$$V_{1,e} = V(0) = V^+(1+\Gamma) \tag{2.18b}$$

With Γ being the reflection coefficient at port one looking towards the normalised load of value 2:

$$\Gamma = \frac{2 - Z}{2 + Z} = \frac{2 - \sqrt{(2)}}{2 + \sqrt{2}} \tag{2.19}$$

By substituting V^+ in equation 2.18b with V^+ from equation 2.18a and using equation 2.19:

$$V_{1_e} = \frac{V_0}{j(1 - \Gamma)}(1 + \Gamma) = -jV_0(-\sqrt{2}) = jV_0\sqrt{2} \tag{2.20}$$

With this all interesting parameters in the even mode circuit is extracted and attention is turned towards the anti-symmetric excitation, the odd-mode. With similar reasoning as with the even mode excitation a bisection can be made out of the circuit in figure 2.13b. This is because of the voltage null appearing between the $r/2$ resistors and in the short circuit between the the inputs of the two transmission lines at port 1. The bisected network can be observed in figure 2.14b. Starting with $Z_{in,o}$ and noticing that the load is a short circuit with a $\frac{\lambda}{4}$ transmission line, resulting in: $Z_{in,o} = \infty$. Thus, if port 2 is to be matched for odd mode excitation: $r/2 = 1 \Rightarrow r = 2$. Furthermore with $Z_{in,o} = \infty$ and $r = 2$:

$$V_{2,o} = \frac{r/2}{r/2 + 1} \cdot 2V_0 = V_0 \tag{2.21a}$$

$$V_{1,o} = 0 \tag{2.21b}$$

Concluding that for the even mode excitation all power is delivered to the resistors, none to port 1.

With the information extracted so far, most of the scattering parameters can be computed. But first the input impedance at port one when ports two and three are terminated in matched loads must be calculated, this is to be able to determine S_{11} The resulting circuit can be seen in figure 2.15a, and similar to the case with even mode excitation: $V_2 = V_3$ which allows for a bisection seen in figure 2.15b.

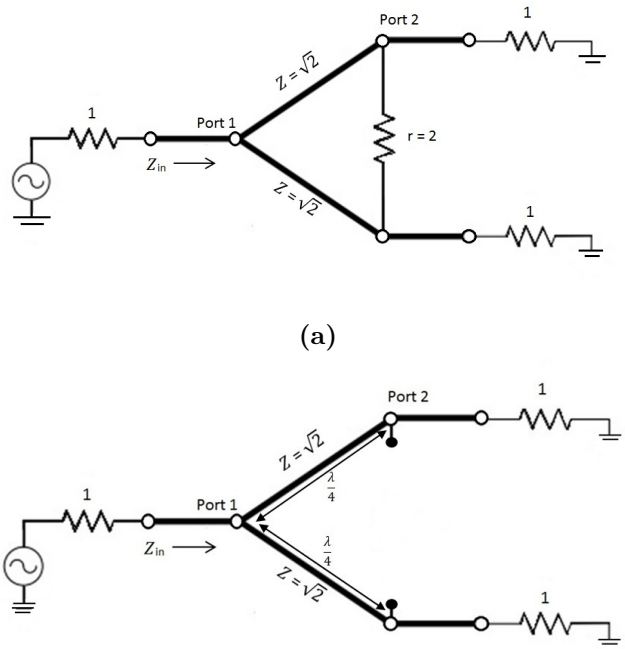

Figure 2.15: Schematic representation of the Wilkinson power divider with ports two and three terminated in matched loads (a) Circuit (b) Bisection of the circuit in (a)

The input impedance, Z_{in}, is that from a parallel connection of two quarter wave transformers with matched loads:

$$Z_{in} = Z \parallel Z = (\sqrt{2})^2 \parallel (\sqrt{2})^2 = 1 \tag{2.22}$$

Meaning that the input at port one is matched. Also it can be noted that the effects of the resistor no longer appear so this circuit is ideally lossless when matched at both output ports.

Finally, the S-parameters of the Wilkinson power divider can be determined, by using equation 2.22 and assuming that all ports are matched, $\Gamma_i n = S_{11}$:

$$S_{11} = \frac{Z_{in} - Z_0}{Z_{in} + Z_0} = 0 \tag{2.23}$$

To obtain a circuit with a voltage source only applied to port two, one can add the even- and odd-mode excitation circuits together from figure 2.13b which will lead to

$V_{g2} = 4V_0$ and $V_{g3} = 0V$. Adding together all the voltages and currents in the two circuits, resulting in:

$$S_{22} = \left.\frac{V_{2,e}^- - V_{2,o}^-}{V_{2,e}^+ + V_{2,e}^+}\right|_{V_1^+=V_3^+=0} \tag{2.24}$$

By selecting $Z = \sqrt{2}$ earlier in the even-mode analysis so that port two was matched, meaning that $V_{2,e}^- = 0$. And in similar fashion in the odd-mode analysis $r = 2$ was selected to match port two, meaning $V_{2,o}^- = 0$ and using equation 2.24 above: $S_{22} = 0$, and by symmetry $S_{33} = S_{22} = 0$.

Continuing with S_{21} and S_{12}, and applying the same procedure as earlier with excitation at port two by adding the even- and odd-mode circuits together. By definition:

$$S_{12} = \left.\frac{V_1^-}{V_2^+}\right|_{V_1^+=V_3^+=0} \tag{2.25}$$

Since port one is matched in both circuits $V_{1,e}^+ = V_{1,o}^+ = 0$ the total voltage at port one is just V_1^-:

$$V_1^- = V_1 = V_{1,e} = V_{1,o} \tag{2.26}$$

Same reasoning applies for V_2^+ since port two is matched:

$$V_{2,e}^- = V_{2,o}^- = 0 \tag{2.27a}$$
$$V_2^+ = V_2 = V_{2,e} = V_{2,o} \tag{2.27b}$$

Consequently, using 2.27 together with the earlier results for $V_{1,e/o}$ and $V_{2,e/o}$ from 2.18 and 2.21:

$$S_{12} = \frac{V_{1,e} + V_{1,o}}{V_{2,e} + V_{2,o}} = \frac{-jV_0\sqrt{2} + 0}{V_0 + V_0} = -j\frac{\sqrt{2}}{2} \tag{2.28}$$

Due to reciprocity: $S_{21} = S_{12}$. And using a similar approach for S_{13} and S_{31} as that for S_{12} and S_{21} one can show:

$$S_{13} = -j\frac{\sqrt{2}}{2} = S_{31} \tag{2.29}$$

And finally for S_{32} and S_{23}:

$$S_{32} = \left.\frac{V_3^-}{V_2^+}\right|_{V_1^+=V_3^+=0} = \frac{V_{3,e}^- - V_{3,o}^-}{V_{2,e}^+ + V_{2,e}^+} \tag{2.30}$$

From earlier odd- and even-mode analysis we know that: $V_{3,e}^- = V_{2,e}^-$ and $V_{3,o}^- = -V_{2,o}^-$. These relations in combination with 2.30, 2.18 and 2.21 conclude that:

$$S_{32} = \left.\frac{V_{2,e}^- - V_{2,o}^-}{V_{2,e}^+ + V_{2,o}^+}\right|_{V_1^+=V_3^+=0} = \frac{V_0 - V_0}{V_0 + V_0} = 0 = S_{23} \tag{2.31}$$

And with this last result one can see that at the design frequency the two output ports are completely isolated from eachother. In summary, the following scattering parameters for the Wilkinson power divider in figure MAKE FIGURE were established:

$$S_{11} = 0 \tag{2.32a}$$
$$S_{22} = S_{33} = 0 \tag{2.32b}$$
$$S_{12} = S_{21} = \frac{-j}{\sqrt{2}} \tag{2.32c}$$
$$S_{13} = S_{31} = \frac{-j}{\sqrt{2}} \tag{2.32d}$$
$$S_{23} = S_{32} = 0 \tag{2.32e}$$

2.3 Broadband Matching

Broadband matching refers to the technique of applying matching networks at all ports of the directional couplers to achieve greater bandwidths. The initial idea was developed by G.P. Riblet where the external network consisted of a quarter-wavelength transformer shunted by half-wavelength open stub [14]. This did improve the bandwidth but the single quarter-wave transformer used, results in very impractical impedances on the lines, in the range of 6 to 8 in reference to the normalised characteristic admittance. The bandwidth is defined as the frequency band of which the isolation and return loss of the device are under a certain level.

Almost a decade later this approach was re-invented by applying two quarter-wave transformers at each of the four ports on a directional coupler, sacrificing the match at center frequency for two matched points at either side of the design center frequency with a slight mismatch at the center frequency. By controlling this mismatch greater bandwidth can be achieved by keeping the isolation and return loss below a predetermined level [15]. The admittances, figure 2.16 for each transmission line in the new broadband hybrid were first extracted for the hybrid ring in [15] by setting up expressions for the eigenadmittances to calculate the eigenreflections and with that the return loss coefficient.

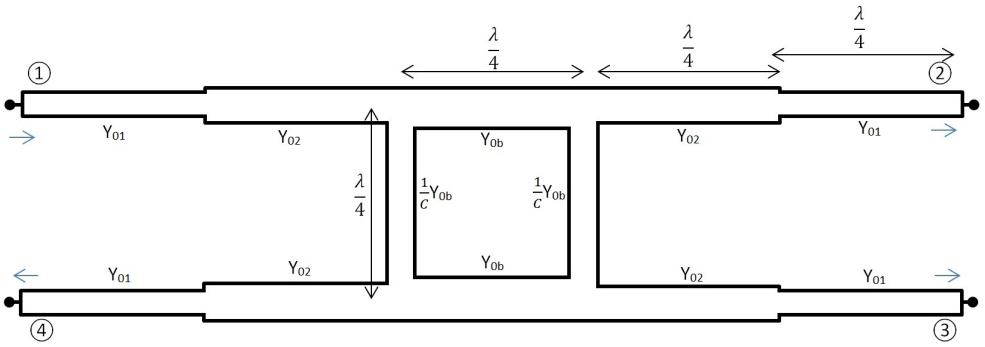

Figure 2.16: Broadband single section branch line coupler with normalised admittances [16].

This technique was later reviewed and applied to the branch line coupler and some design equations regarding the line admittances were constructed [16]. The analysis was done by taking the even- and odd-mode circuits and imposing a condition on each of the circuits: at two equidistant frequencies from the designed center frequency the load impedance would be transformed to a real value at the center points of the circuits. Applying this to either one of the circuits is enough [16]. The design equations that emerged were:

$$0 = [(1+V)\cos^2(\Delta) - (1+\frac{1}{V})\sin^2(\Delta)]Y_{01}^2 + [\frac{1}{\cos(\Delta)}]\frac{1+C}{1-C}Y_{01} \tag{2.33a}$$
$$- [(1+V)\cos^2(\Delta) - (1+V)\sin^2(\Delta)]$$

$$Y_{0b} = \frac{C}{1-C^2}[\frac{\cos(\Delta)}{(\sin^2(\Delta) - V\cos^2(\Delta))^2 + \frac{(1+V)^2\sin^2(2\Delta)}{4Y_{01}^2}}] \tag{2.33b}$$

The reflection coefficient at center frequency is given as:

$$\Gamma(f_0) = \frac{(\frac{1}{C^2} - 1)(Y^2 - \frac{1}{Y^2})}{4 + (\frac{1}{C^2-1})(Y + \frac{1}{Y})^2} \tag{2.34a}$$

Where C is the coupling coefficient and $V = \frac{Y_{01}}{Y_{02}}$ and $Y = V^2(\frac{1-C^2}{C})Y_{0b}$ and the two normalised frequencies chosen for zero reflection:

$$f_1 = \frac{90 - \Delta}{90} \tag{2.35a}$$

$$f_2 = \frac{90 + \Delta}{90} \tag{2.35b}$$

By fixing Δ and the admittance ratio V one can find several solutions and choose the ones that can easiest be realised for the chosen transmission line solution, i.e. microstrip. An interesting discovery was made when $V = 1$, resulting in half-wavelength matching sections [16]. This is a very practical result from a fabrication point of view because it means that junction discontinuities can be avoided between the two quarter-wavelength sections, also setting $\Delta = 0$ resulted in a maximally flat solution which results in a hybrid with a perfect match at center frequency but with twice the bandwidth [16].

This procedure was further improved when it was discovered that cascading another half-wavelength section could further improve the bandwidth while maintaining flat amplitude characteristics [17]. The same paper also showed that similar results could be achieved by attaching a half-wavelength open stub instead, resulting in a quadruple bandwidth increase for a single section branch line hybrid.

2.4 Fabrication

Method of fabrication regarding microwave devices is a very wide and vast topic, this section will cover the principles of the chosen method for the devices proposed in this thesis which are of planar structure, i.e. microstrip or stripline. The devices will be fabricated using standard circuit board processes used in industry for easy and fast production and integration with other systems. Initially the process steps will be explained and finally the limitations of the method will be discussed.

The photolithography process is widely used in the semiconductor industry due to low cost, speed and simplicity. There are methods to achieve much greater precision in fabrication: E-beam lithography, X-Ray lithography, Ion beam lithography and so on, but manufacturing times and costs tend to escalate. The process consists of three basic steps: deposition/growth, patterning and etching (note that etching can be replaced by a lift-off process in some situations).

The process starts with the chosen circuit board material, the substrate. In this case it is the Rogers RO4350B laminate made out of woven glass and reinforced hydrocarbon/ceramics. These boards are often called ”laminates” because the dielectric material is bonded to a thin copper layer on one or both sides of the dielectric. This allows for having patterning on one side and a ground plane on the other which can be connected by through-holes. This leads to the first process step which is making holes in the board, this is to able to mount certain components and to make vias or through-holes. The holes are drilled mechanically and the vias have a diameter of 0.3 mm in this work.

Next the board needs have the conducting copper pattern deposited, this is done by electroplating, it requires that the parts that are supposed to be covered to be electrically conductive. Which means that the holes need to be covered in some thin ($\sim 2\mu m$) copper layer first, this is often done in one of the following two ways: chemical deposition or direct metallisation/hole conductivisation [18]. Once the holes are conductive the board is ready for the copper deposition by electroplating.

Electroplating is a deposition process that works like a reversed galvanic cell, an electric current reduces metallic cations from a solution and coats a conductive surface with a thin layer of the metal. A simple illustration of the process can be seen in figure 2.17. The conductive surface to be coated acts as a cathode in the circuit and the metal to be plated as anode. Both the anode and cathode are immersed in an electrolyte solution containing the desired metal to be plated in the form of ions as well as other ions to allow for electric flow through the circuit. Direct current is applied to the anode, causing an oxidation of its metal atoms and dissolving them in the electrolyte solution. The dissolved metal ions are then reduced at the cathode and it gets ”plated” by the metal. The current through the circuit is of a magnitude so that the rate of which the anode is dissolved is the same as the rate of which the cathode is plated[1]. This briefly explains the basic principles of electroplating, but there are two different types of plating processes used: pattern plating and panel plating. The two processes differ in the way the board is prepared before the electroplating and in the after-treatment, both with their advantages and disadvantages.

[1]This is true to some extent, in practice there is a time dependency since the concentration of ions in the solution decreases over time due to evaporation and it has to be restored to keep the balance between the plating and dissolving of the anode. And it is not applicable to all metals, gold plating is somewhat a different process than copper plating.

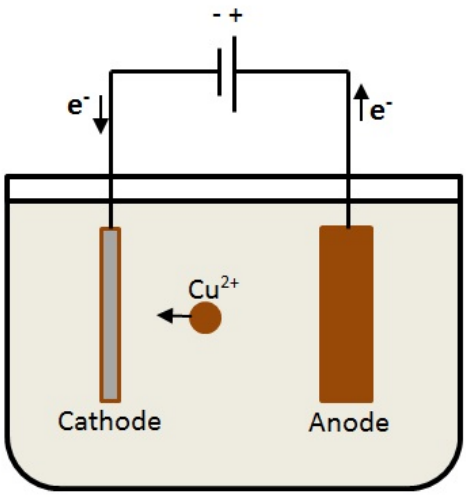

Figure 2.17: A simplified illustration of the electroplating process.

If we start with the more common pattern plating process it starts with covering the whole board with a photoresist layer, afterwards the photoresist is exposed to radiation (most often UV-light) through a mask creating the circuit pattern in the resist. The resist is then developed creating a "canyon" exposing the surface copper in the desired circuit pattern. Another copper layer is then deposited by electroplating until sufficient thickness is achieved, the resist now works as a plating-resist allowing only for copper to be plated on the surfaces that are conducting, i.e., that are not covered by resist. Once a thick enough layer has been achieved an etch-resist needs to be deposited on top of the exposed copper layer, this is often done by electroplating a thin layer of tin or led ($\sim 4-15\mu m$) [18], this is because the etchant does not affect the tin/led layer and thus it protects the underlying copper. Once the tin/led layer has been deposited the remaining photoresist is stripped away and the base copper layer that was hidden underneath is then etched away leaving the etchresist covered copper layer. As a final step the etchresist layer is stripped away making sure that only the desired copper pattern and plated holes are left on the circuit board. The process steps for pattern plating are illustrated in figure 2.18.

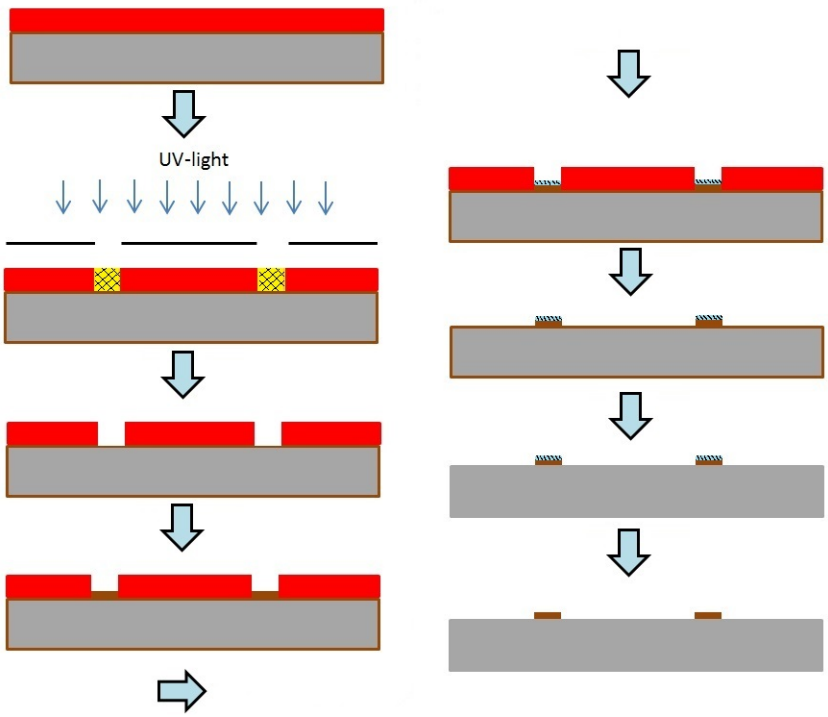

Figure 2.18: A flow chart of the pattern plating process described in the text.

The panel plating process is very similar to pattern plating, but instead of coating the board with resist before the electroplating, the whole board is electroplated with desired copper thickness. After the electroplating, then a photoresist is applied on top and developed to cover the desired circuit pattern and holes like an etch-resist. In a final step after the photoresist is radiated and developed the surrounding copper is etched away. Once the copper is etched away the remaining photoresist is removed and the desired copper pattern together with the plated holes are all that remains. The process flow can be seen in figure 2.19.

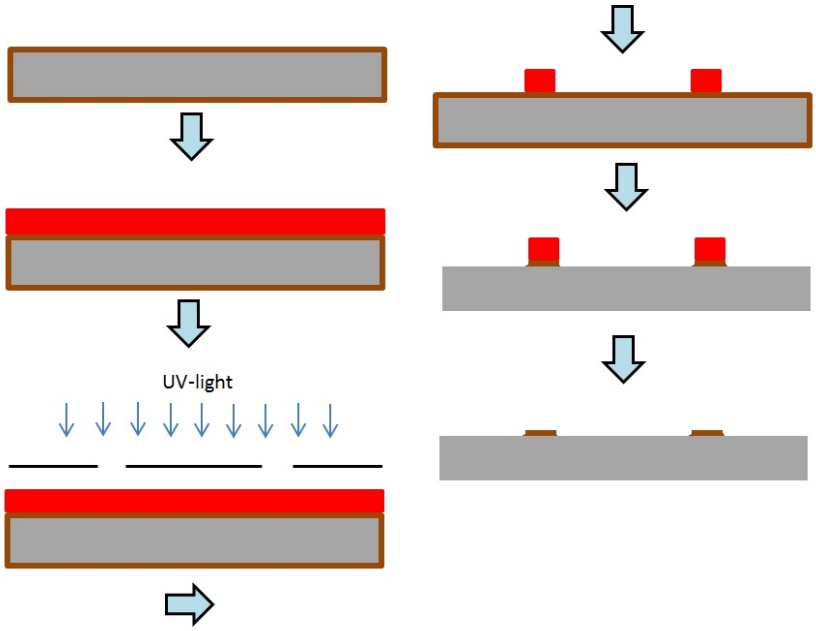

Figure 2.19: An illustration showing the panel plating process step by step.

The main advantages with panel plating are less process steps and the ability to create a uniform copper layer, important in microwave applications. Since panel plating avoids all the steps involving tin or led plating it is often less time consuming. But because of the larger surface area that is getting copper plated one needs to use much higher currents in the electrolyte bath and the amount of copper used is considerably higher. Also the thicker layer of copper that needs to be etched away in the panel plating process contributes to greater under-etching which increases the minimum achievable width for the conductors [18], a figure illustrating the effect of under-etching can be seen in figure 2.20.

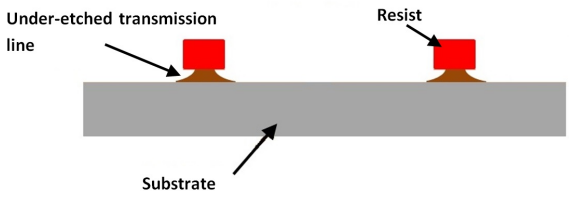

Figure 2.20: An illustration of the under-etching phenomena often occurring in the panel plating process.

3

Quadrature Hybrid Designs

This chapter will present the design methods used to create the quadrature hybrids, i.e. the branch line hybrids. The devices all follow the same procedure starting with software simulation and optimisation. All devices designed in this thesis are simulated and fabricated on the same substrate: Rogers TM4350B, with a thickness of 10 mil or $254\mu m$, $\epsilon_r = 3.66$ and a loss tangent of 0.002.

3.1 Simulations

The designs and computer simulations were done using Advanced Design Systems (ADS) from Agilent Technologies for all devices.

3.1.1 Branch Line Couplers

The first part of the project was to design branch line hybrids for wideband operation, four designs will be presented with two different 'core designs' called design A and B. Design A consists of a standard two section branch line hybrid based on impedance values from [6]. This design will work as a reference and comparison to the novel design, design B. Next an impedance matching technique to improve bandwidth as described in section 2.3 was applied to design A. Design B is based on the proposal for a multisection branchguide coupler [19]. Finally the same broadband matching technique as used earlier for design A was applied to design B. All the devices were designed by following the same procedure, so to avoid repeating, the methodology described in the proceeding section is applicable to all cases. All devices are designed with a center frequency of 10 GHz so all mentions of wavelengths are in reference to the center frequency unless stated otherwise.

Design A

This design, as mentioned consists of a two section (or three-branch) branch line coupler, figure 3.1. At first the schematic circuit is created using ideal components, the initial impedance values for the branches and the lines were taken from [6] and then computer optimised towards the imbalance and isolation conditions specified for this project.

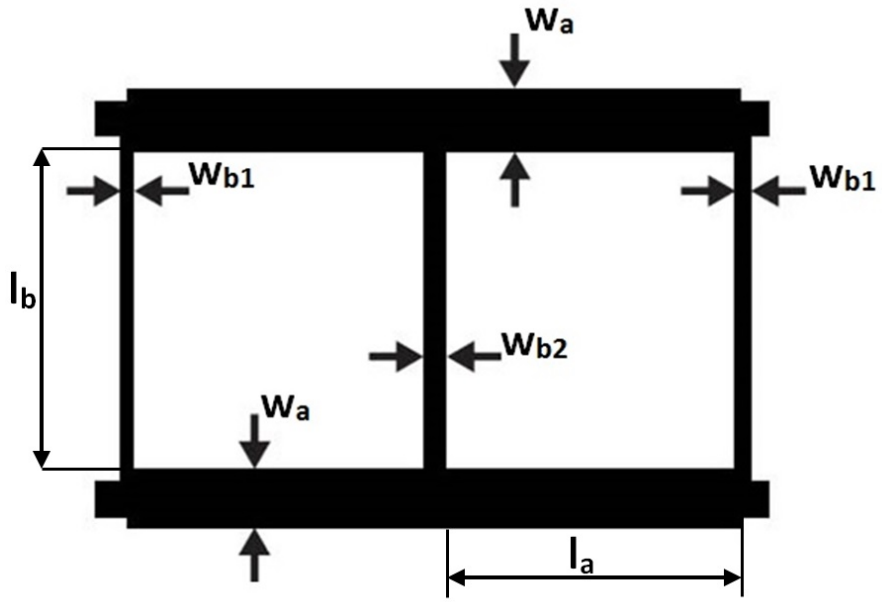

Figure 3.1: Layout for a microstrip two section branch line hybrid.

The theoretical results can be observed in figures 3.2a and 3.2b.

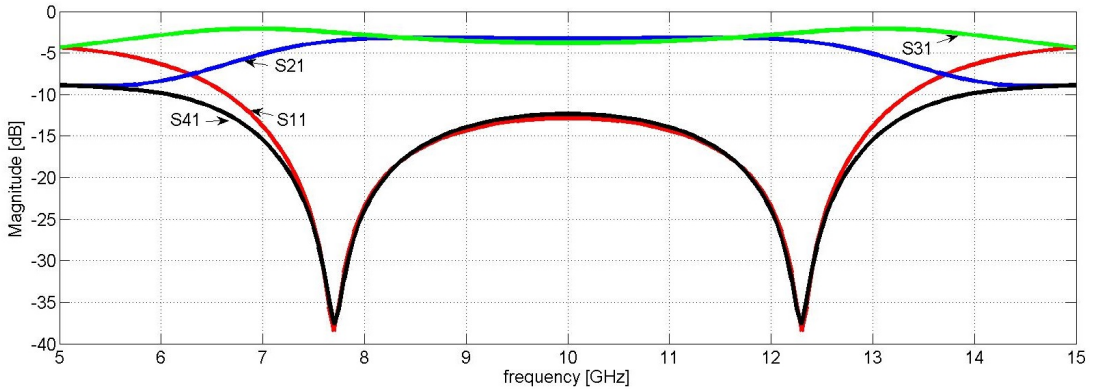

(a)

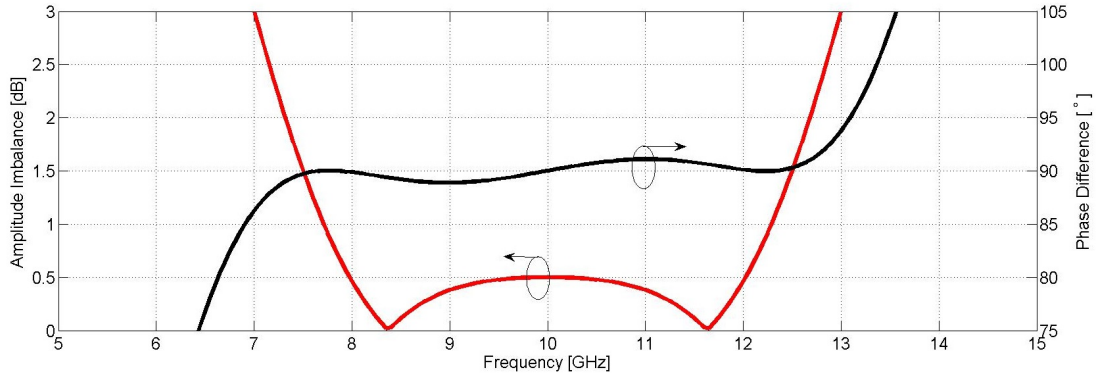

(b)

Figure 3.2: Theoretical results assuming lossless lines for the standard 2 section BLC (Design A). (a) S-parameters. (b) Amplitude imbalance and phase difference between the two output ports

Next the impedance values of the ideal transmission lines were synthesised to length and width values for microstrip lines on the chosen substrate by using the *Linecalc* tool in the software. The thickness of the substrate was chosen based on the resulting impedance values after optimisation, this is because of the relation between substrate thickness and the width of the microstrip transmission lines. The fabrication limits govern the minimum line width (maximum impedance) which is set to 0.2 mm (0.15 mm can be accepted in some cases) and the maximum width (minimum impedance) is decided by the quarter wavelength of the top frequency in the bandwidth. The width should ideally not exceed $\frac{\lambda}{8}$ at the top frequency. The final geometrical parameters as denoted in figure 3.1: $w_a = 0.88\ mm, w_{b1} = 0.2\ mm, w_{b2} = 0.32\ mm, l_a = 4.28\ mm, l_b = 4.68\ mm$

Final part of the simulation stage is the 2.5D Electromagnetic (EM) simulation, performed with the Momentum tool in ADS. A Computer Aided Design (CAD) layout is generated from the microstrip schematics and some mitering is done where appropriate according to [1]. This is to minimize the parasitic capacitance to ground-plane due

to the relatively large area at these intersections. The problem with large junction discontinuities due to big differences in impedance values of the transmission lines was relieved by mitered sections. The final circuit-dimension of the device is: 6.5 by 9.1 mm.

Design A with Broadband Matching

The broadband matching consists of matching networks at each port as described in section 2.3. By setting the branch line hybrid impedances to fixed values (using the ones from Design A) and thereafter tuning the stub impedances one can achieve proper 'mismatch'. The stubs create reflection zeros at equal distance on both sides of the original perfectly matched points which can be seen in the resulting plots or with a Smith chart representation. See section 2.3 for further analysis.

The final layout of this quadrature hybrid is presented in figure 3.3. The final geometrical parameters as denoted in figure 3.3: $w_a = 0.92\ mm, w_{b1} = 0.2\ mm, w_{b2} = 0.40\ mm, l_a = 5.29\ mm, l_b = 4.58\ mm, w_s = 0.44\ mm, l_s = 9.28\ mm, w_p = 0.17\ mm, l_p = 9.73\ mm$. Resulting final circuit-dimension is 25.4 by 29.9 mm. Theoretical performance is simulated and illustrated in figures 3.4a and 3.4b. The minimum transmission line width condition was relieved a bit to allow for a higher impedance for the open stubs at each port, the higher impedance was required to achieve optimal performance.

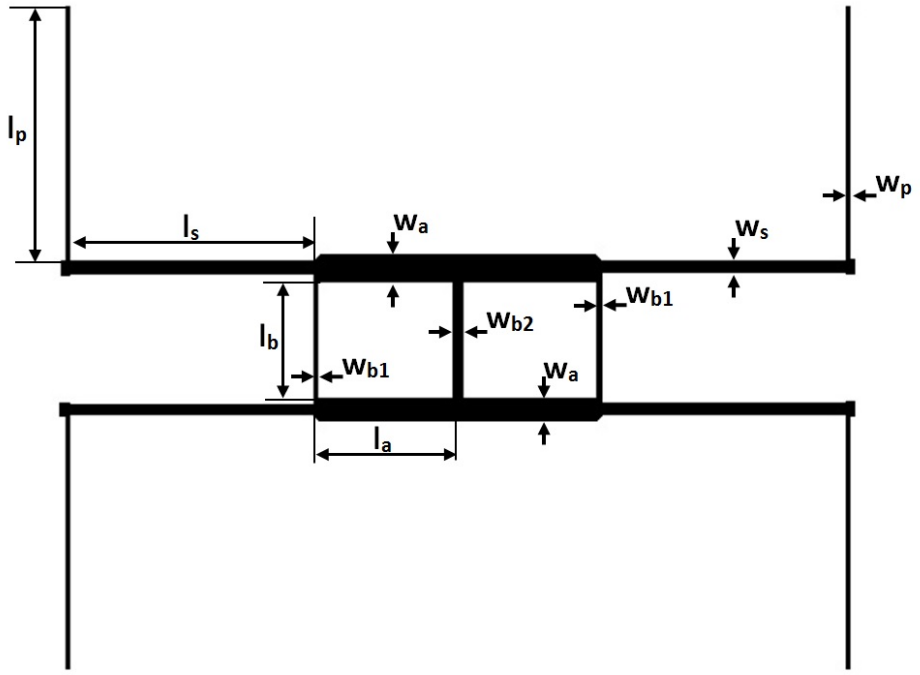

Figure 3.3: Layout for a microstrip two section branch line hybrid with a broadband matching network at each port.

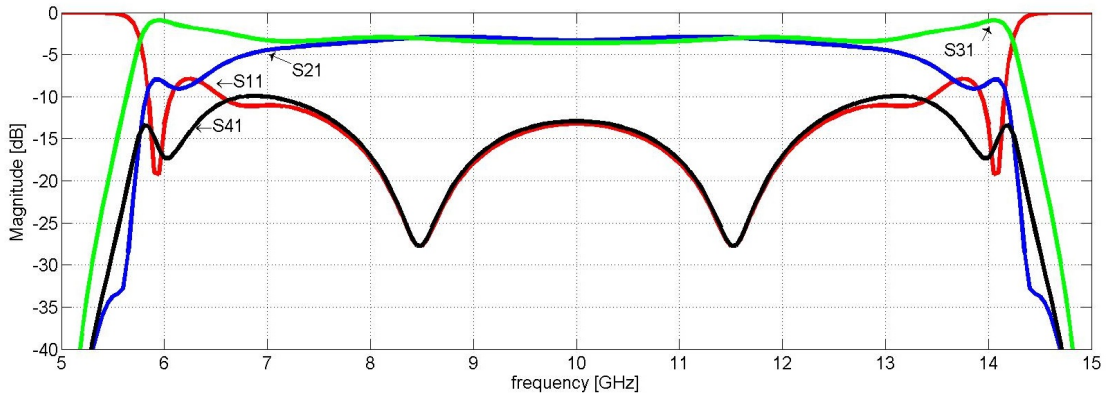

(a)

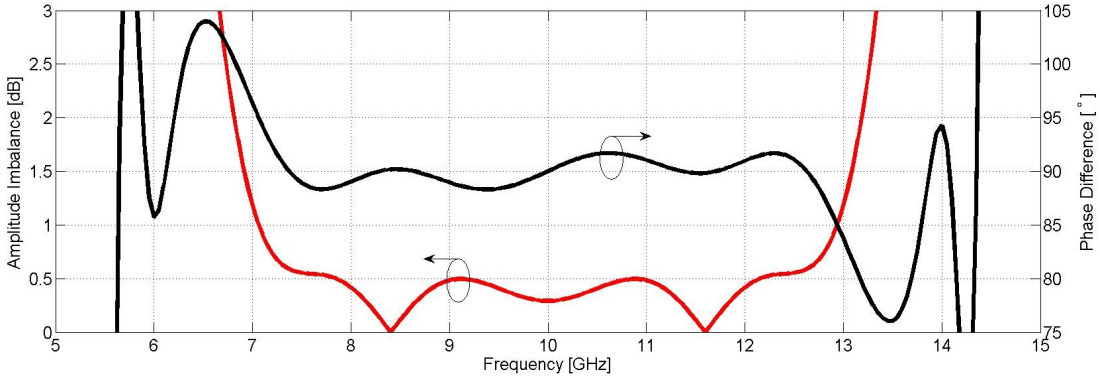

(b)

Figure 3.4: Theoretical results assuming lossless lines for the standard 2 section BLC (Design A). (a) S-parameters. (b) Amplitude imbalance and phase difference between the two output ports

Design B

Design B as mentioned is based on the waveguide hybrid proposed in [19]. Briefly explained it consists of two multi-section 8.34 dB couplers cascaded together, creating a 3 dB coupler. This is a well-known method to achieve 3 dB coupling, an example can be seen in [20] with two 8.34 dB single section BLC, but the interconnecting line was half a wavelength long and of same impedance as the other line, at center frequency the half wavelength lines have no effect on impedances. The proposal by [19] arguments for a quarter wavelength interconnecting line with an impedance that differs from the other lines as well as from the input impedance, creating small reflections and thus small ripples in the transmission characteristics. The resulting effect is that very low amplitude imbalance can be achieved over a great bandwidth, example can be seen in the proceeding subsection *Design B With Broadband matching*. The two 8.34 dB couplers were made from two-section BLCs, more sections would result in a better bandwidth

but the impedance values of the out-most branches are too high to be realised. Even with a two-section hybrid the basic impedance needed to be lowered to 25Ω due to manufacturing constraints. To solve this problem an additional three stage Chebychev transformer for 25Ω to 50Ω port impedance was employed and folded to minimize the circuit size. A three stage Chebychev was chosen so that the bandwidth would not be reduced due to the transforming section. The bandwidth for a N-step Cebychev impedance transformer with f_c center frequency can be calculated with equation 3.1, where Γ_m is the chosen maximum value of reflection coefficient over the passband [1].

$$\frac{\Delta f}{f_0} = 2 - 4\frac{\sec^{-1}(\cosh[\frac{1}{N}\cosh^{-1}(\frac{ln(Z_L/Z_0)}{2\Gamma_m})])}{\pi} \tag{3.1}$$

The resulting layout can be seen in figure 3.5, geometrical dimensions as noted in the figure are: $w_{t1} = 0.55\ mm, l_{t1} = 4.51\ mm, w_{t2} = 0.64\ mm, l_{t2} = 4.07\ mm, w_{t3} = 1.06\ mm, l_{t3} = 2.95\ mm, w_{a1} = 2.17\ mm, w_{a2} = 1.56\ mm, w_{b1} = 0.2\ mm, w_{b2} = 0.33\ mm, l_{a1} = 3.83\ mm, l_{a2} = 4.23\ mm l_b = 4.19\ mm$, giving a total circuit size of 16.9 mm by 37.0 mm.

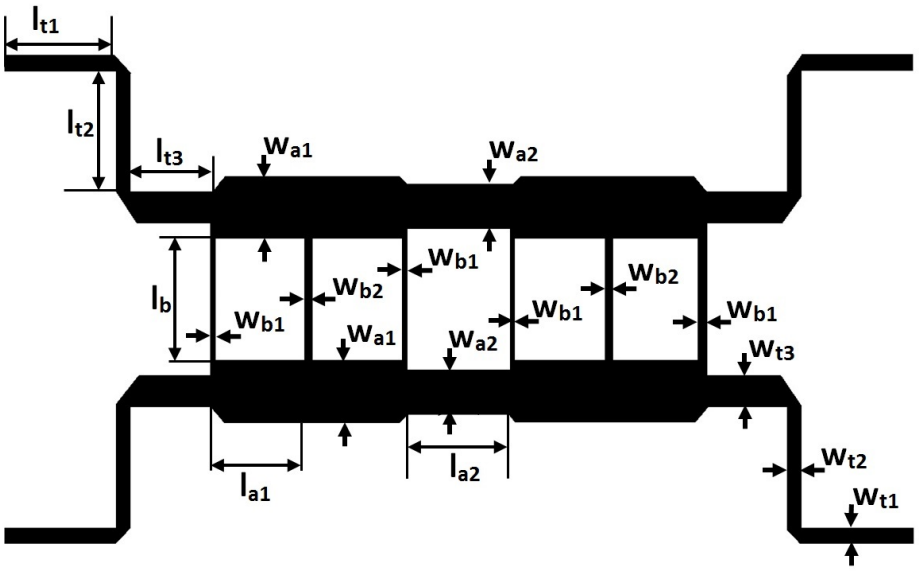

Figure 3.5: Layout for a novel microstrip branch line hybrid, design B, with a three stage Chebychev transformer at each port.

The initial impedance values for the 8.34 dB couplers were taken from [5] and then computer optimised towards the desired specifications. The theoretical performance can be observed in figure 3.6.

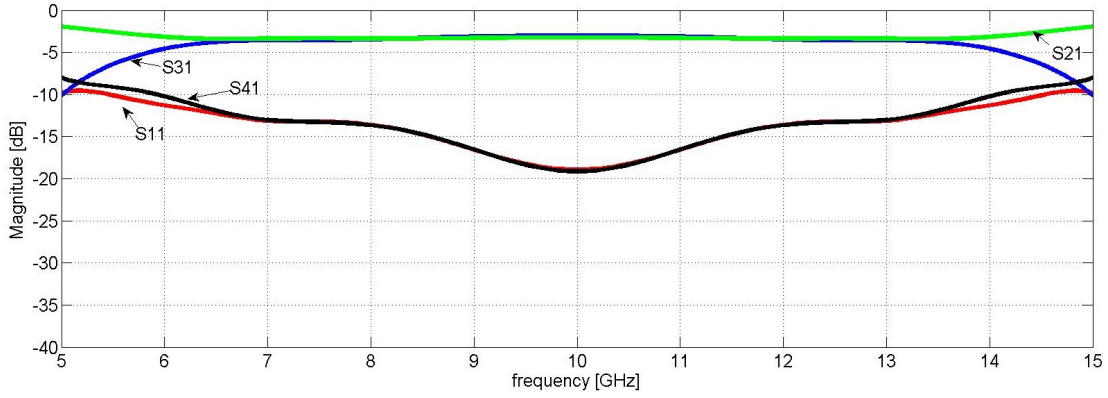

(a)

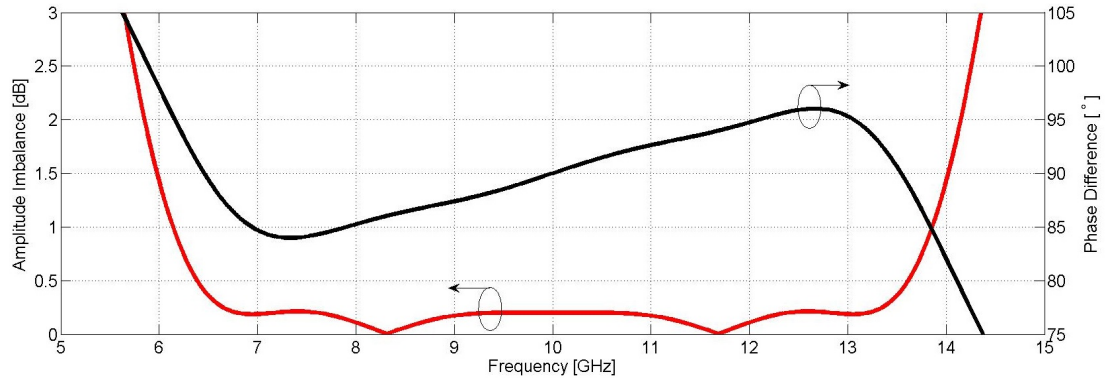

(b)

Figure 3.6: Theoretical results assuming lossless lines for the novel design (Design B). (a) S-parameters. (b) Amplitude imbalance and phase difference between the two output ports

Design B With Broadband Matching

The final design proposal is based on the core structure described in the previous section *Design B* together with the matching stub network at each port of the structure. As expected there was an increase in bandwidth compared to the structure in *Design B*. In this design the manufacturing constraints again were relieved a bit by allowing the open stubs go below the initially set minimum of 0.2 mm to about 0.15 mm. The final layout is illustrated in figure 3.7, geometrical dimensions as denoted in the figure:$w_{t1} = 0.47\ mm, l_{t1} = 4.49\ mm, w_{t2} = 0.55\ mm, l_{t2} = 4.07\ mm, w_{t3} = 0.97\ mm, l_{t3} = 3.74\ mm, w_{a1} = 2.15\ mm, w_{a2} = 1.55\ mm, w_{b1} = 0.2\ mm, w_{b2} = 0.25\ mm, l_{a1} = 4.1\ mm, l_{a2} = 4.29\ mm l_b = 4.29\ mm, w_s = 1.13\ mm, l_s = 8.34\ mm, w_p = 0.15\ mm, l_p = 9.34\ mm$, with a total circuit-dimension of 26.3 by 56.3 mm.

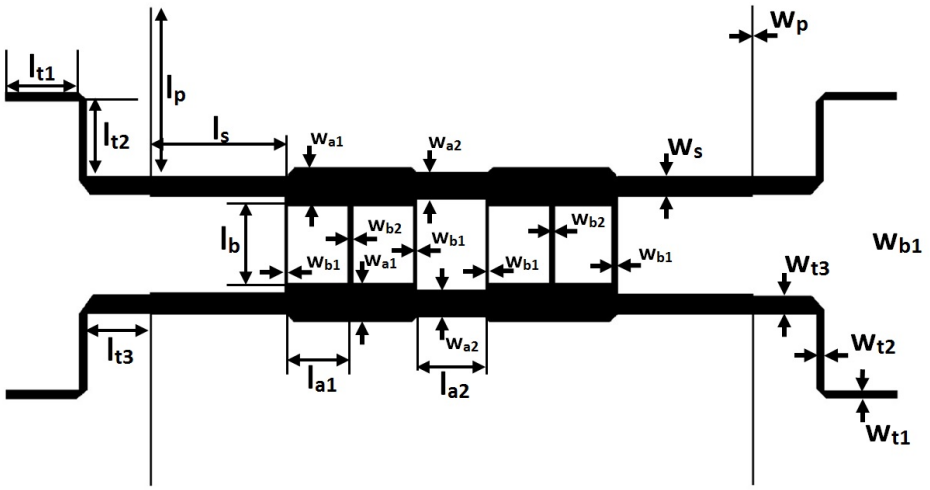

Figure 3.7: Layout for a novel microstrip branch line hybrid, design B, with a broadband matching network and a three stage Chebychev transformer at each port.

As mentioned in the preceding section this designs allows for great performance regarding the amplitude imbalance. By relieving constraints for return loss and phase imbalance theoretically amplitude imbalance below 0.03 dB can be achieved, figure 3.8. But since the focal point of this work is bandwidth the amplitude imbalance conditions were relieved for better bandwidth. The theoretical performance of the final device broadband matching networks can be seen in figure 3.9

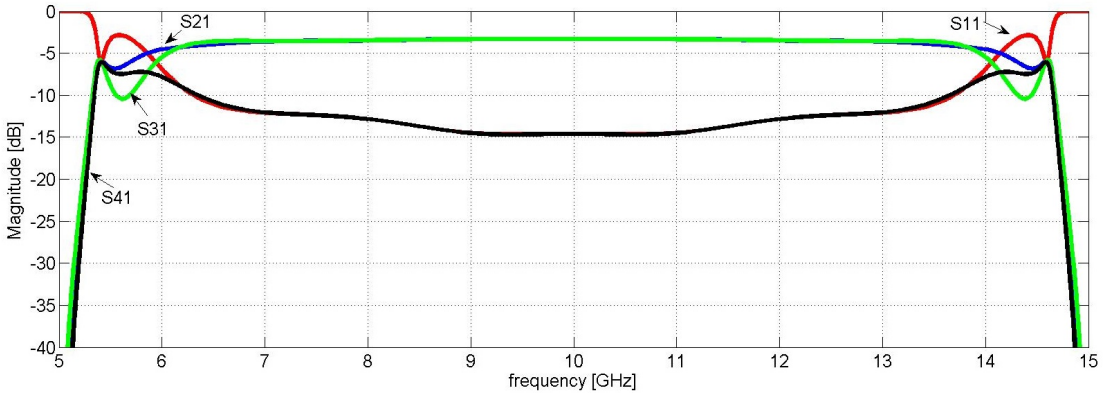

(a)

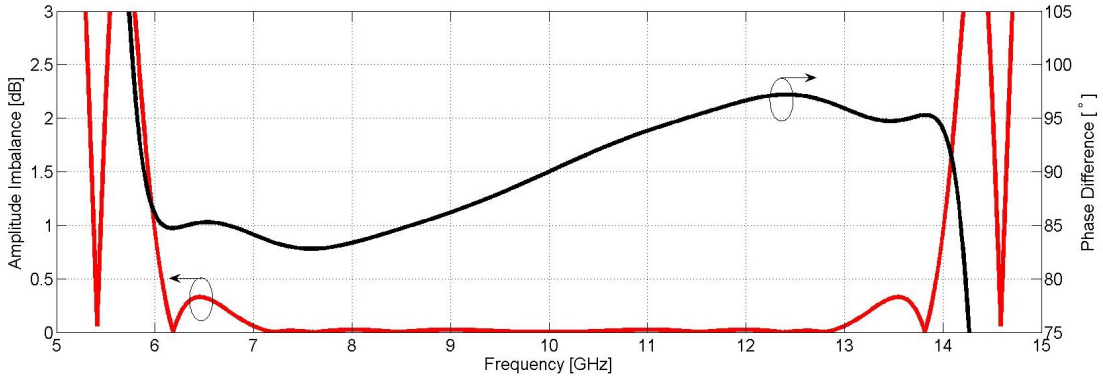

(b)

Figure 3.8: Theoretical results assuming lossless lines for the novel design (Design B) optimised towards extremely flat amplitude characteristics. (a) S-parameters. (b) Amplitude imbalance and phase difference between the two output ports

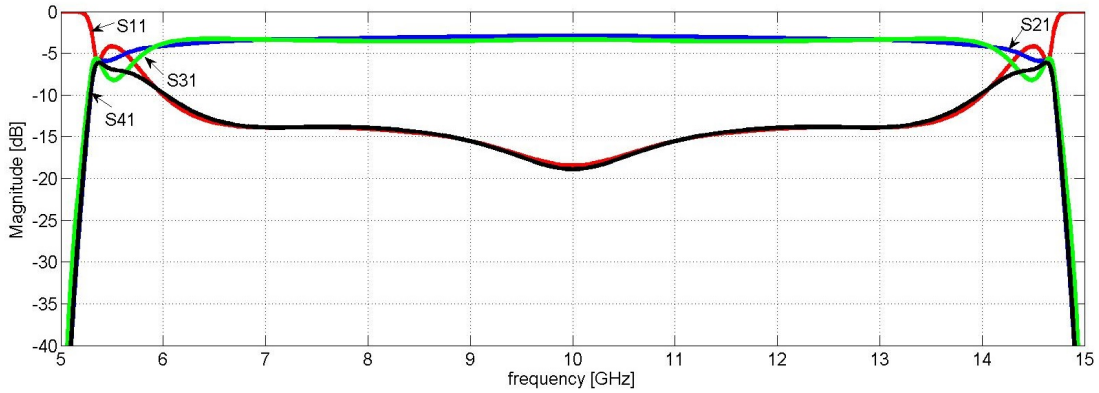

(a)

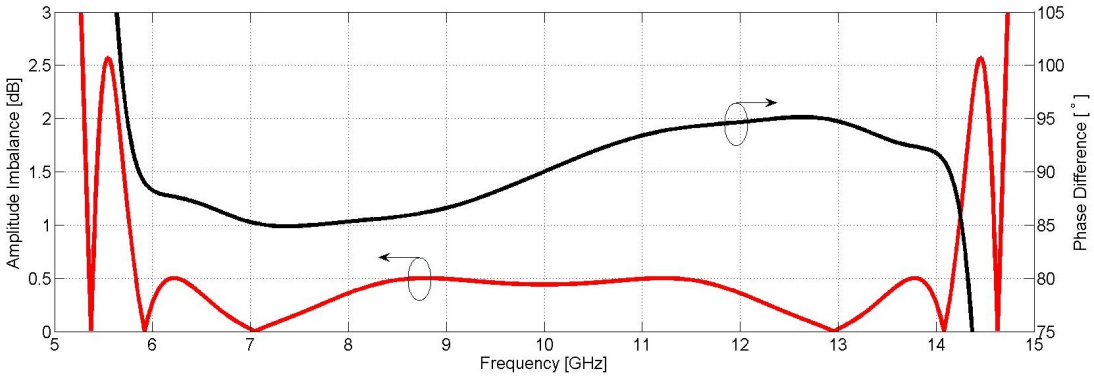

(b)

Figure 3.9: Theoretical results assuming lossless lines for the novel design (Design B) optimised towards bandwidth. (a) S-parameters. (b) Amplitude imbalance and phase difference between the two output ports

4

180 Degree Power Splitter Design

This chapter aims to describe the design process of the proposed 180 degree power splitter. The device consists of two separate sections: a power divider and a phaseshifter. The power divider is a multi-stage Wilkinson power divider based on the equations from [13], and the phaseshifter is made entirely in microstrip based on a delay line and phase stabilising T-section with short circuited stubs [21]. Three devices were constructed, the final out of phase splitter as well as the two components making the device, this was to make individual measurements and analyses possible. All devices are designed for a center frequency of 10 GHz so when wavelengths are mentioned in the following sections of this chapter it is in reference to the center frequency unless stated otherwise.

4.1 Simulations

All designs and computer simulations were as before done in ADS. This section will briefly describe the design process and show the theoretical performance for the three devices starting with the equal split Wilkinson power divider.

4.1.1 Wilkinson Power Divider

The Wilkinson power divider is a well-known and well-studied device initially proposed in 1960 by Ernest J. Wilkinson [22], and developed almost a decade later by Seymour B. Cohn [13]. Cohn introduced the multi-section Wilkinson power divider and the impedance values for the transmission lines and resistors used in this thesis are taken from the ones synthesised by Cohn. The power divider is very well matched, with a VSWR (Voltage Standing Wave Ratio) close to unity making it very easy to combine with other devices. The power divider designed in this work consists out of four sections can theoretically provide a 160% bandwidth with an isolation and return loss better than 13 dB, figure 4.2. The $\lambda/4$ (at a center frequency of 10 GHz) transmission lines at each section are bent to minimise circuit area and to avoid coupling between the two lines due

to the small dimension of the resistors used (0,04 × 0,02 inch thick-film chip-resistors), the final microstrip layout is illustrated in figure 4.1. Performance in terms of scattering parameters over a wide frequency band, assuming lossless lines is presented in figure 4.2

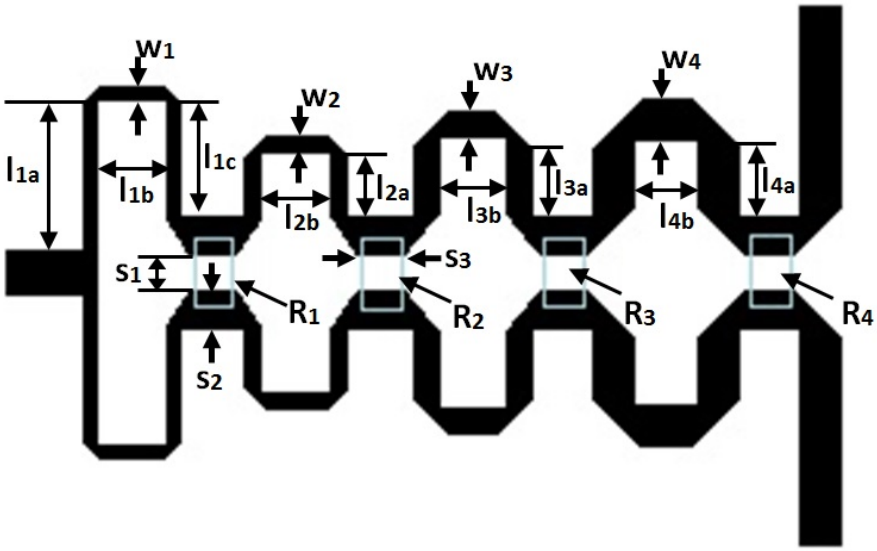

Figure 4.1: Microstrip layout for the 4-section Wilkinson power divider

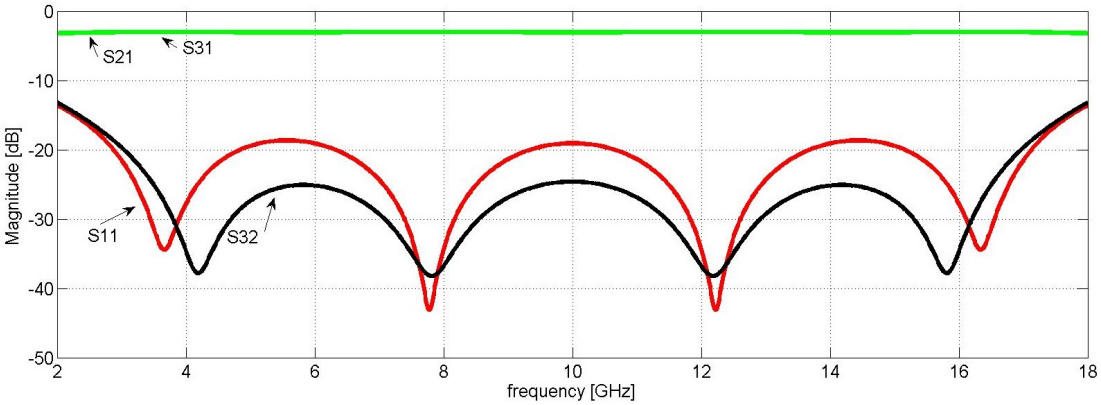

Figure 4.2: Performance for the four-section Wilkinson equal split power divider assuming lossless lines.

The geometrical dimension that emerged after optimisation: $w_1 = 0.18\ mm, l_{1a} = 1.72\ mm, l_{1b} = 0.79\ mm, l_{1c} = 1.31\ mm, w_2 = 0.22\ mm, l_{2a} = 0.67\ mm, l_{2b} = 0.79\ mm, w_3 =$

$0.33\ mm, l_{3a} = 0.79\ mm, l_{3b} = 0.78\ mm, w_4 = 0.51\ mm, l_{4a} = 0.79\ mm, l_{4b} = 0.73mm, s_1 = 0.38\ mm, s_2 = 0.5\ mm, s_3 = 0.55\ mm$. The resistor values are as follows: $R_1 = 100\ \Omega, R_2 = 180\ \Omega, R_3 = 330\ \Omega, R_4 = 470\ \Omega$. All parameter names are in reference to figure 4.1.

4.1.2 Phaseshifter

The phaseshifter used consists of two sections: a 50Ω transmission line with electrical length $N \cdot \lambda_c/2 + \lambda_c/2$ at the center frequency of $10GHz$, section between ports 1 and 2 in figure 4.3, and a grounded shunt $\lambda_c/4$ transmission line section with impedances Z_{shunt} and Z_{series} to control phase response and improve return loss respectively, section between ports 3 and 4 in figure 4.3 [21]. At center frequency the grounded shunt stubs have an insertion phase of 0° and the two series $\lambda/4$ lines have an insertion phase of 180°, consequently this section provides an insertion phase of 180°. These two sections are then attached to one output port each of the wideband power divider providing a phase difference between the output ports of $N \cdot 180^\circ + 180^\circ - N \cdot 180^\circ = 180^\circ$. Careful selection of the impedance values Z_{shunt} enables the phase of the two outputs ports to be aligned, achieving a broadband constant phase shift. Increasing the number of section improves return loss and phase imbalance, however with the cost of increasing circuit size as well as very high stub impedances [21]. An analysis of the T-network in the phase shifter can be seen in Appendix A.

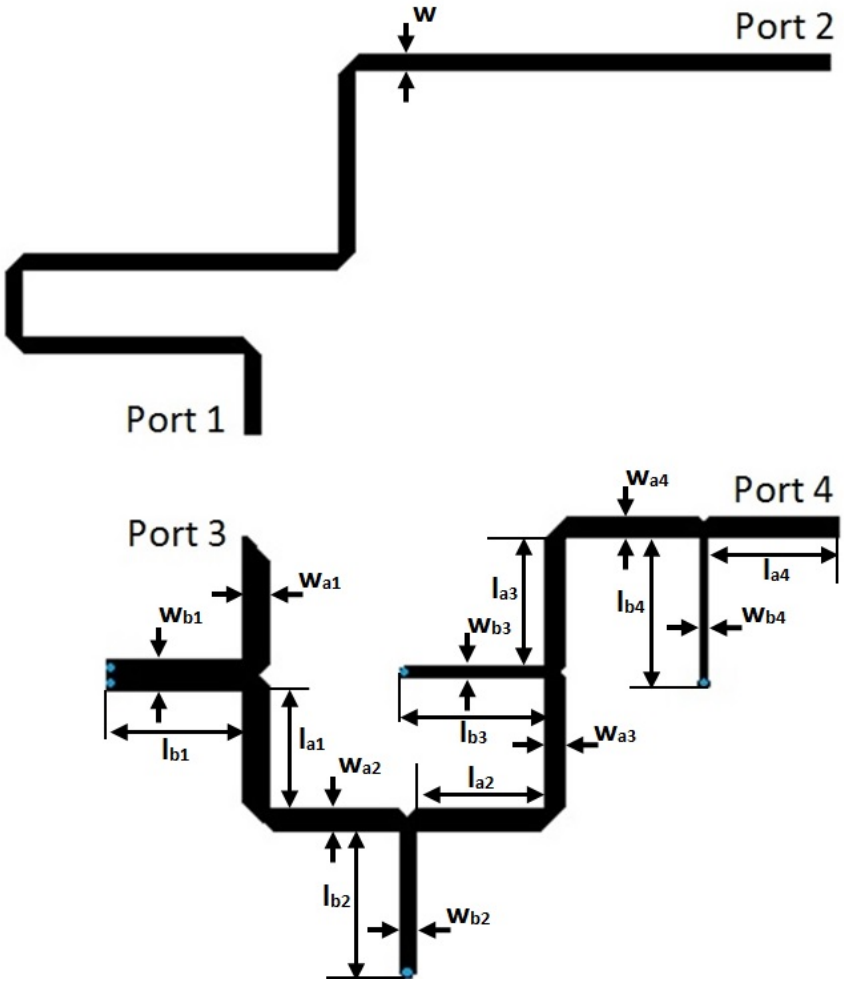

Figure 4.3: Microstrip layout for the 180 degree phaseshifting network, the stubs from port 3 to port 4 are shorted stubs.

The theoretical performance for the 180° is presented in figure 4.4. On a side note the upper line is intentionally unfolded compromising smaller circuit area to fit selected measurement contacts, so a smaller circuit size is possible. The geometrical dimensions as noted in figure 4.3: $w = 0.54\ mm, w_{a1} = 0.94\ mm, l_{a1} = 3.70\ mm, w_{b1} = 1.00\ mm, l_{b1} = 4.29\ mm, w_{a2} = 0.79\ mm, l_{a2} = 4.06\ mm, w_{b2} = 0.57\ mm, l_{b2} = 4.66\ mm, w_{a3} = 0.71\ mm, l_{a3} = 4.08\ mm, w_{b3} = 0.4\ mm, l_{b3} = 4.59\ mm, w_{a4} = 0.67\ mm, l_{a4} = 4.24\ mm, w_{b4} = 0.25\ mm, l_{b4} = 4.80\ mm$ where the total length of the delay-line is approximately $44mm$ which is approximately two and a half wavelengths at the center frequency (10 GHz).

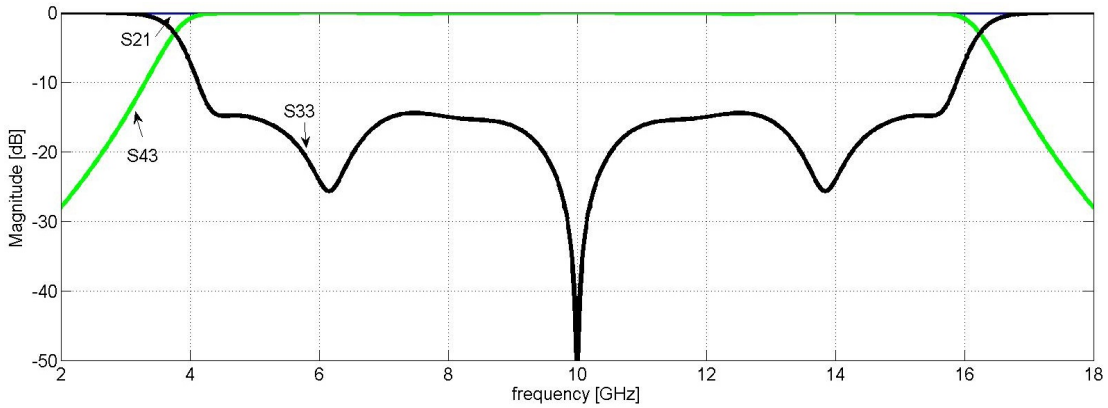

(a)

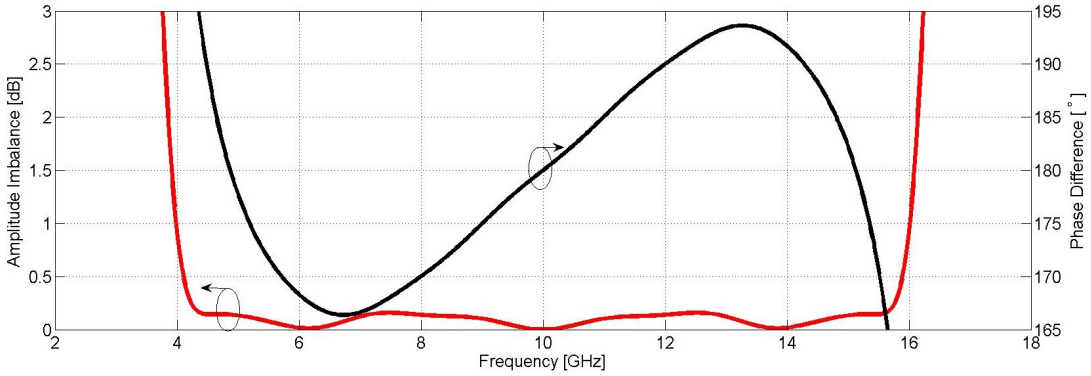

(b)

Figure 4.4: Theoretical results assuming lossless lines for the phaseshifting network. (a) S-parameters. (b) Amplitude imbalance and phase difference between the two output ports

4.1.3 180 degree power splitter

Finally the two separate circuits are combined to form an out-of-phase power splitter, the geometrical dimensions of the power divider and the phase shifting section are the same as presented in the earlier sections for the separate devices. No further tuning was needed insinuating that both circuits are well-matched. The final size of the 180 degree power splitter is 27.4 mm by 29.1 mm, and it should be noted that the circuit size could easily be made smaller by folding the delay line of the phase shifting section but it was intentionally left unfolded for reasons stated earlier. The geometry of this design compares well with current microstrip rat-race hybrid designs, which are approximately of the same size but with a substantially smaller fractional bandwidth [23, 24].

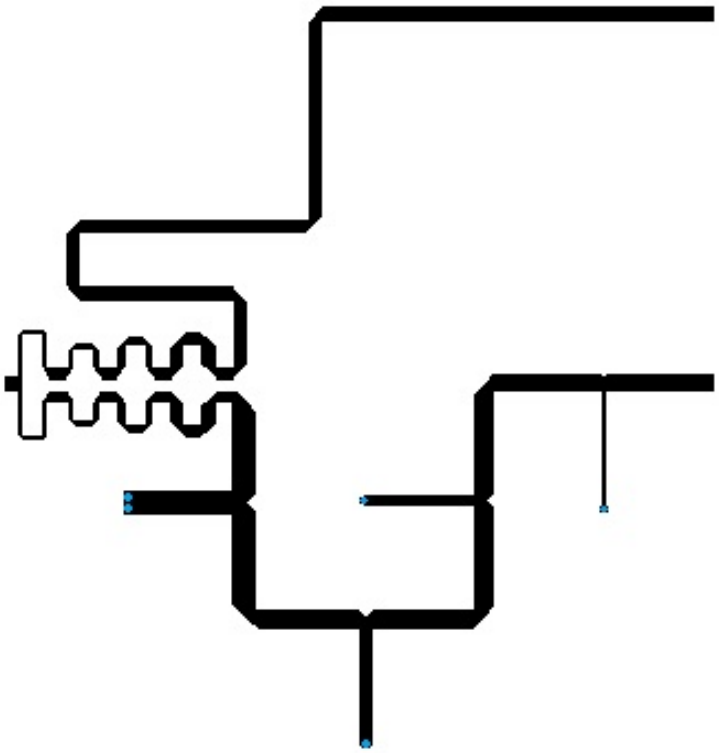

Figure 4.5: Final microstrip layout for the 180 degree power divider.

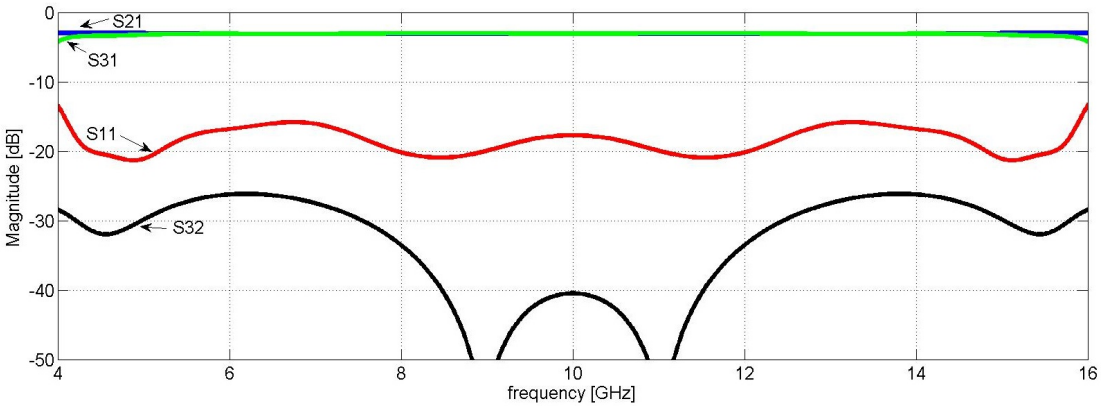

(a)

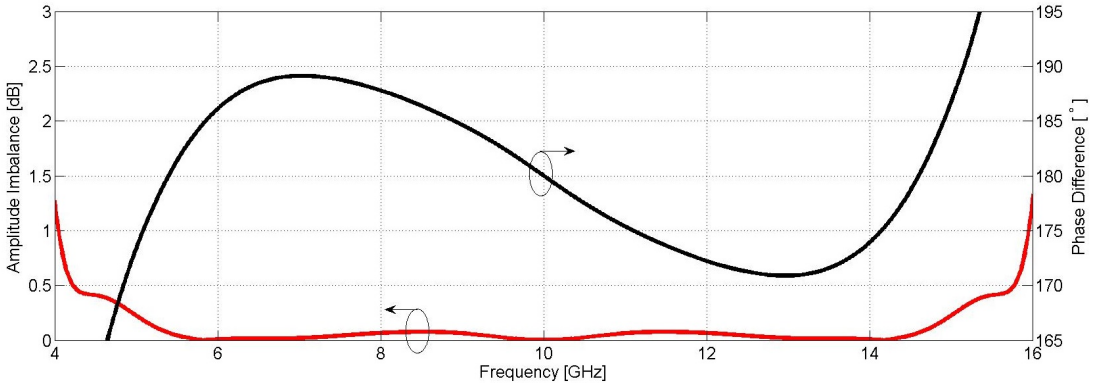

(b)

Figure 4.6: Theoretical results assuming lossless lines for the final 180 degree power divider. (a) S-parameters. (b) Amplitude imbalance and phase difference between the two output ports

5

Results

This chapter will present simulation and measurement results for all of the devices designed in this work. The simulations were carried out in Agilent's ADS Momentum tool, a 2.5D EM simulator. Measurements were performed with a 4-port Vector Network Analyser (VNA) from Agilent Technologies: N5242A PNA-X. A brief description of the measurement procedure will be presented first, followed by the results for the quadrature couplers and the 180° power splitter.

5.1 Measurement Procedure

Measurements were performed by connecting two ports from the Device Under Test (DUT) to the VNA by coax cables (GORE PHASEFLEX [25]). No other apparatus was needed since only passive devices are used and require no external biasing, signal generators and so forth. Even though the VNA had 4-port capability, two port measurements were done due to complications in the 4-port calibration procedure, 50Ω terminations were attached to the two (one for the three port devices) unconnected ports on the DUT. Since the quadrature couplers are of reciprocal/symmetric nature there was no need for a full s-parameter characterisation in the sense that one port at random was used as input port and assuming reciprocity the results would have been the same using any other input port, see section 2.1.1 for further explanation of BLC properties.

The connectors used were of type *End-Launch SMA Connectors* by *Southwest Microwave* attached to the board by screws and require no soldering of the contact pin [26]. An illustration of the setup can be seen in figure 5.1. Regarding calibration, Through-Reflection-Line (TRL) also known as Line-Reflection-Line (LRL) calibration standards were used [1]. The calibration-kit was manufactured on the same substrate as the devices of thesis (Rogers TM4350B, 0.254μm thickness) and employed the same connectors, this is to achieve better accuracy in the measurements than if a standard electronic calibra-

tion (e-cal) would have been used. The TRL calibration also allows for removal of the coax-to-microstrip transition and the parasitic effects of the connector pads.

Due to the fact that all circuit boards were mistakenly delivered with green solder-mask coating it created an extra procedure step in the measurements. The mask was scraped off the transmission lines with a scalpel, the solder-mask layer altered the perceived impedance and length of the lines and thus shifted the center frequency of the devices. It also needed to be removed to enable soldering of the resistors for the Wilkinson power dividers. Because of the simple and primitive way of removing the solder-mask a performance degradation was expected. Measurements were performed both before and after scraping on the quadrature hybrids to investigate the effects, the devices containing Wilkinson power splitters could not undergo measurements before scraping because of the complication with the soldering of resistors.

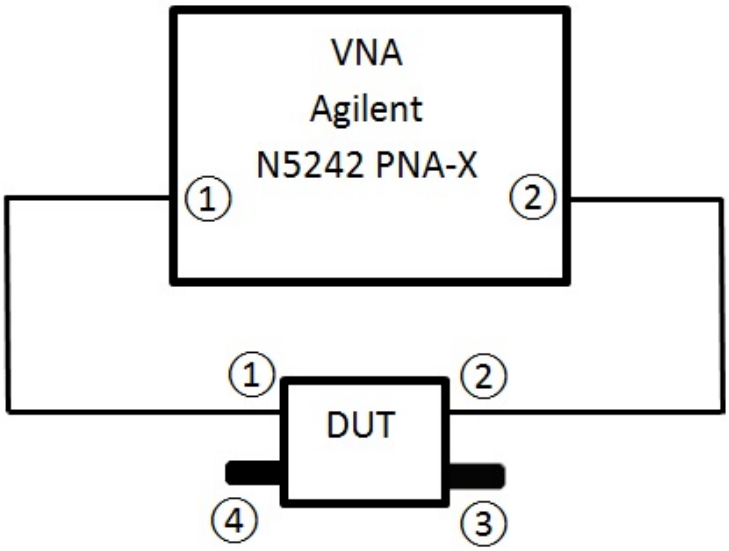

Figure 5.1: Block diagram of the S-parameter measurements performed on the quadrature couplers with ports 1 and 2 connected to the VNA and ports 3 and 4 terminated.

5.2 Branch Line Couplers

The simulation and measurement results will be presented in the form of graphs providing the scattering parameters and phase-/amplitude-imbalances for each device.

5.2.1 Design A

The results from the EM simulations can be seen in figure 5.2 and the measurement results are presented in figure 5.3. The measured performance of the quadrature hybrid

agrees poorly with the simulated performance. This is could be due to complications caused by the scraping of the soldering mask, damaging the underlying copper layer and roughing up the surface. There is most likely also some mask residue left along the edges of the transmission lines causing losses and mismatches. There is certainly some error due to fabrication tolerances which are of IPC Class III, meaning an error of about $\pm 25\mu$m is to be expected. The degradation of performance for the fabricated circuit is probably due to a combination of these stated reasons.

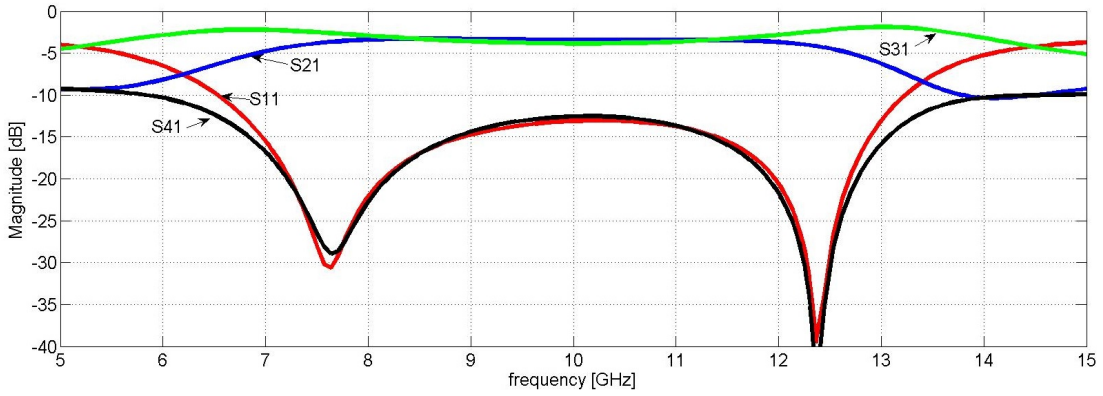

(a)

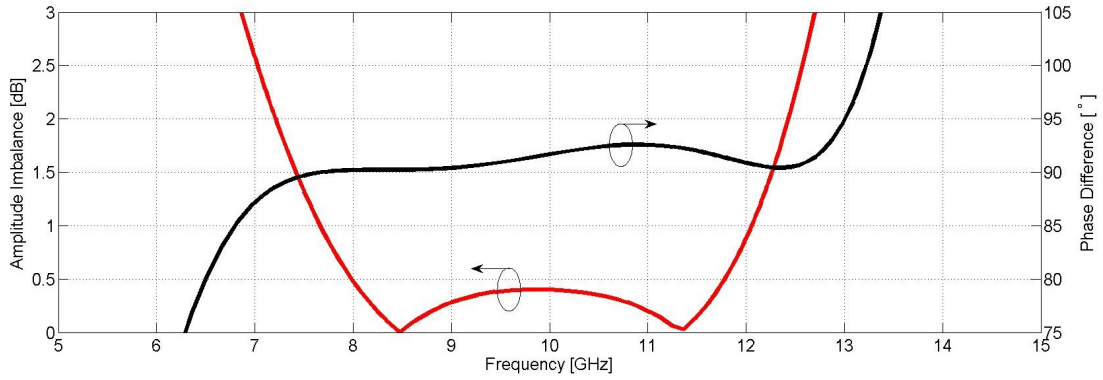

(b)

Figure 5.2: Results after EM simulation (2.5D) in ADS Momentum for the standard 2 section BLC (Design A). (a) S-parameters. (b) Amplitude imbalance and phase difference between the two output ports

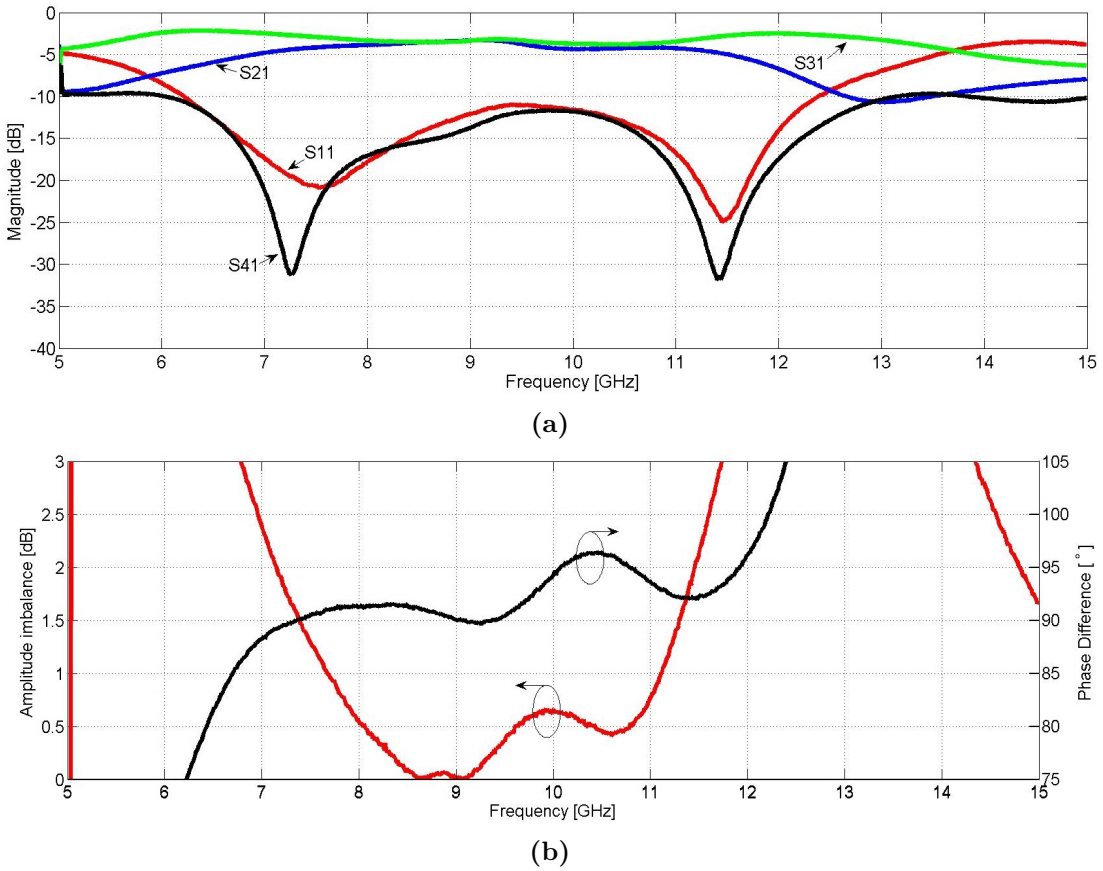

Figure 5.3: Measurement results for the fabricated 2 section BLC (Design A). (a) S-parameters. (b) Amplitude imbalance and phase difference between the two output ports

5.2.2 Design A With Broadband Matching

Figure 5.4 and figure 5.5 illustrate the simulated and measured performance respectively. There is a better agreement than for the previous device between the simulated and measured results. Difference between measured and simulated result are also assumed to be because of reason stated earlier for *Design A*.

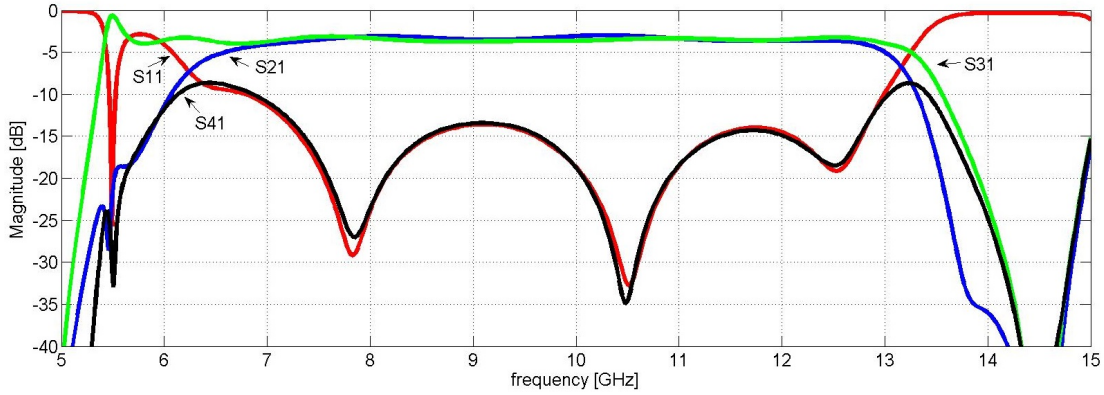

(a)

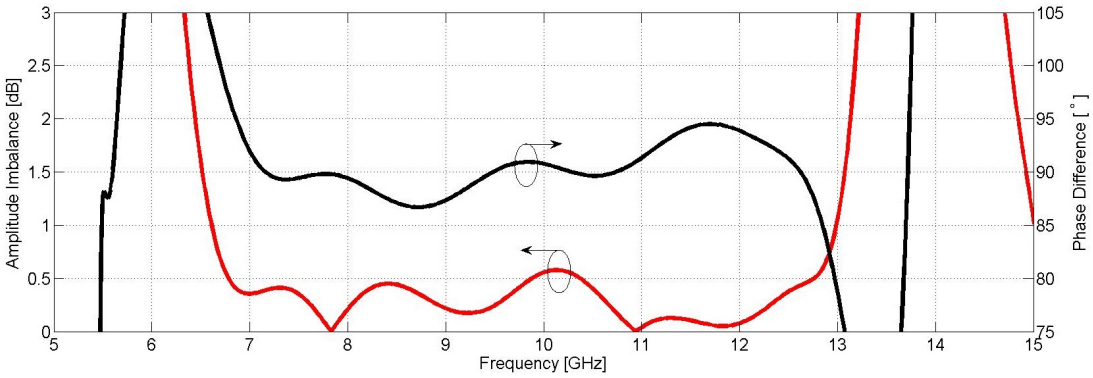

(b)

Figure 5.4: Results after EM simulation (2.5D) in ADS Momentum for the standard 2 section BLC (Design A) with broadband matching networks at every port. (a) S-parameters. (b) Amplitude imbalance and phase difference between the two output ports

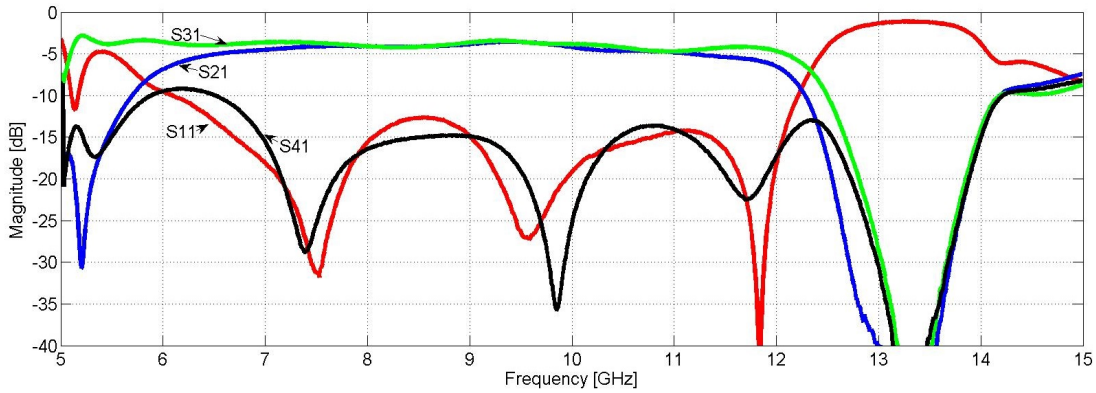

(a)

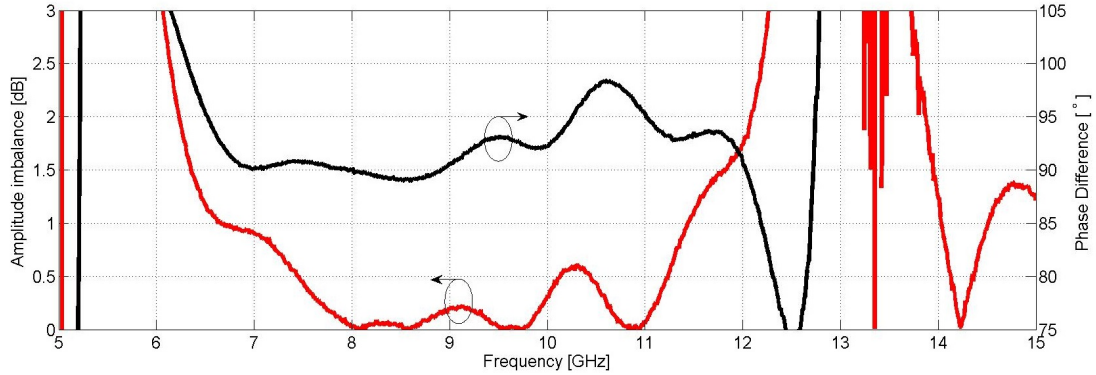

(b)

Figure 5.5: Measurement results for the fabricated 2 section BLC (Design A) with broadband matching networks. (a) S-parameters. (b) Amplitude imbalance and phase difference between the two output ports

5.2.3 Design B

Below, in figures 5.6 and 5.7, the simulated and measured results for the novel quadrature hybrid design can be observed. The measured parameters agree poorly with the simulated ones, but some similarity can be observed.

Reasons behind the results are probably of the same nature as stated for design A but they seem to have a greater effect here. This is most likely because Design B is more sensitive towards changes in line width/lengths, simulations show even a 0.3 mm decrease of the linewidth w_{a1} or an increase by 0.05 mm of w_{b1} will cause an amplitude imbalance increase as the one observed in figure 5.7. Since the fabrication linewidth tolerance is around $\pm 25\mu$m (IPC Class III) it is likely that inaccuracy in fabrication of the high impedance branches is a major influence in the poor measurement results. The shift in center frequency is almost certainly due to an increase in length of the transmission lines causing the desired electrical length of $\lambda/4$ being true for a lower

frequency than the intended one of 10 GHz. The fabrication tolerances in combination with the solder-mask scraping are the most likely cause of performance degradation, it is hard to estimate which one is more prominent but with the results from circuit simulations and the observed sensitivity of the high impedance branches the scraping treatment was most likely not a dominant factor.

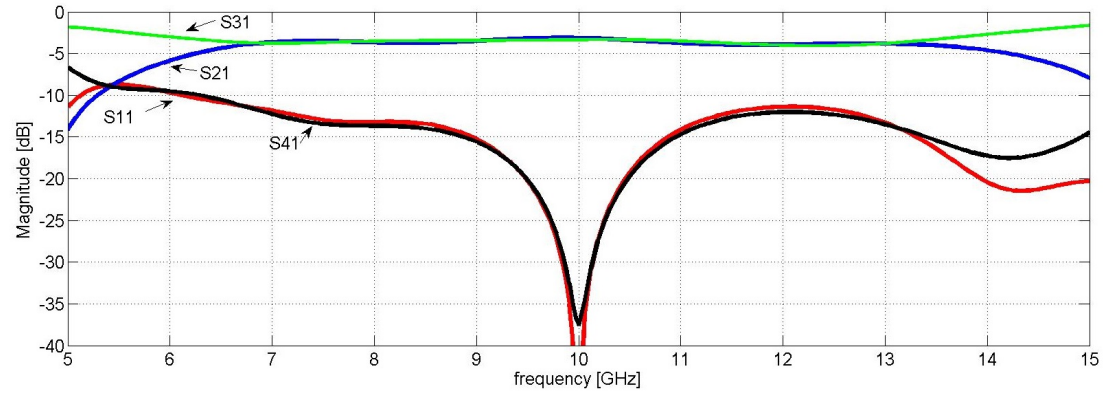

(a)

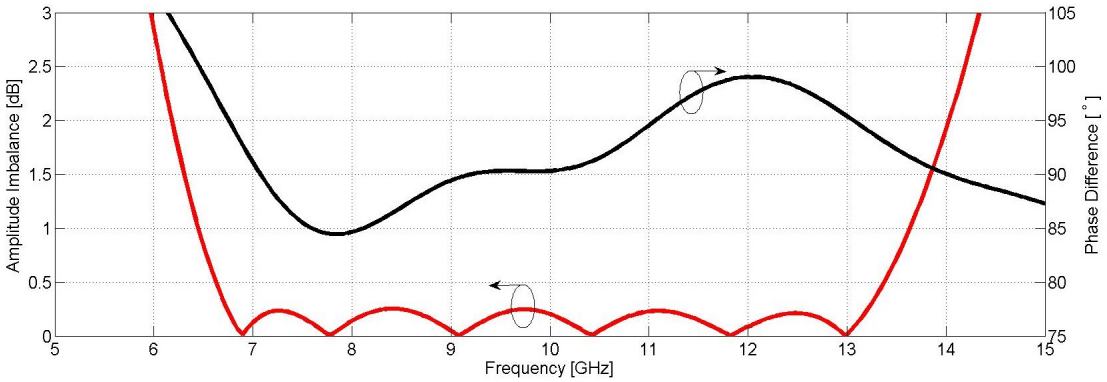

(b)

Figure 5.6: Results after EM simulation (2.5D) in ADS Momentum for the proposed design B. (a) S-parameters. (b) Amplitude imbalance and phase difference between the two output ports

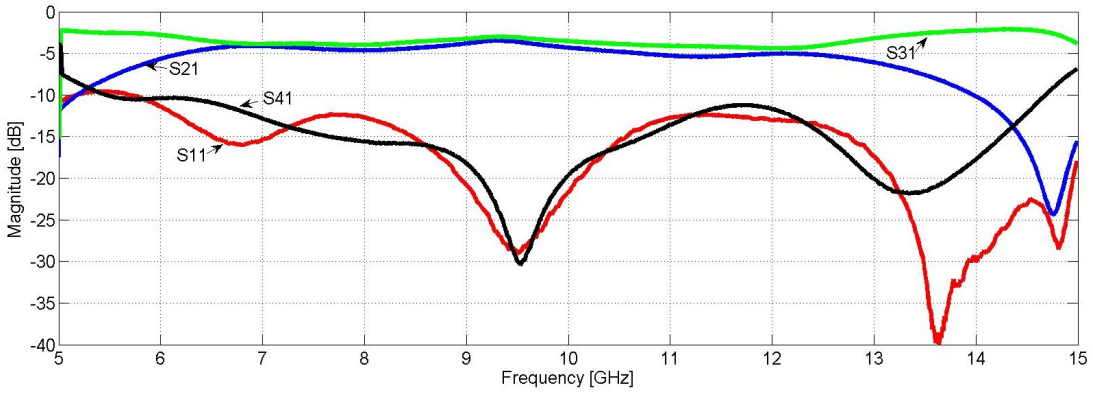

(a)

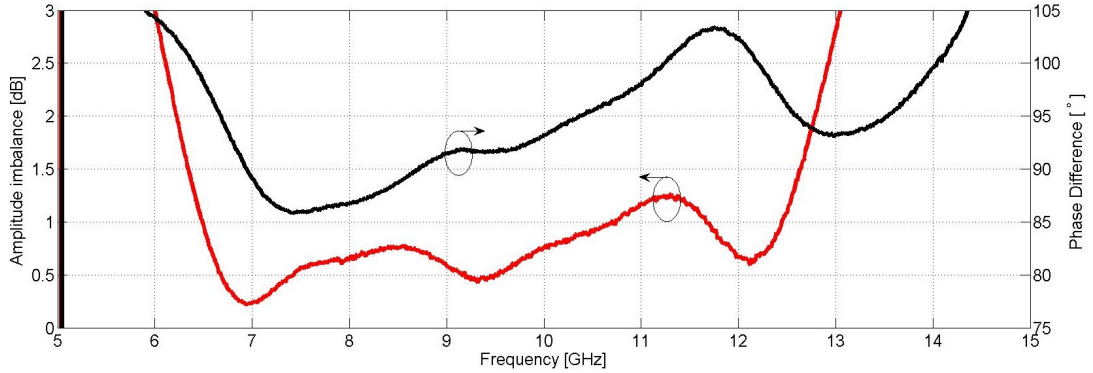

(b)

Figure 5.7: Measurement results for the proposed quadrature hybrid: design B. (a) S-parameters. (b) Amplitude imbalance and phase difference between the two output ports

5.2.4 Design B With Broadband Matching

Summing up the results for the quadrature hybrids, the simulated and measured performance of the novel hybrid: design B with broadband matching networks. Figures 5.8 and 5.9 illustrate the simulated and measured performance respectively. Some resemblance between the simulated and measured results is noticed, also a pronounced frequency shift to the left is observed for the measured device. But the broadband matching networks seem to have an improving effect in reference to the amplitude imbalance comparing the results from *Design B*. The difference in simulated and measured results can be explained with the same reasoning as for the previous device, Design B.

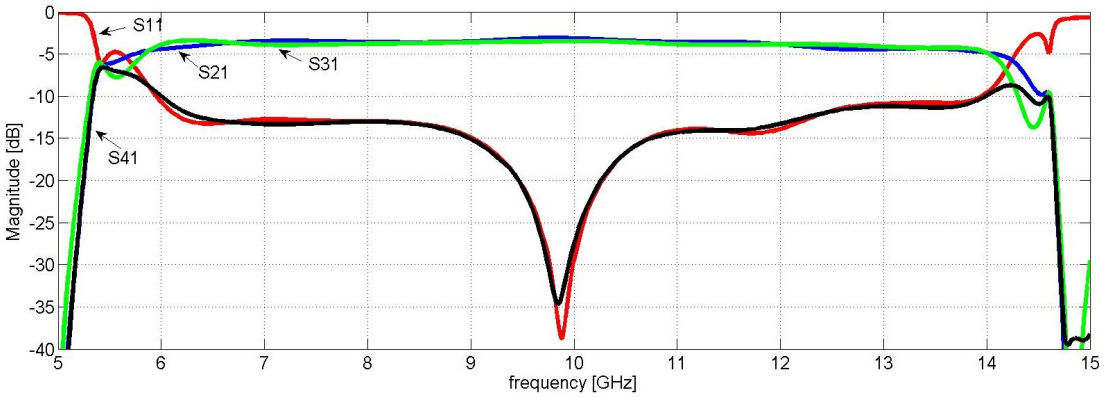

(a)

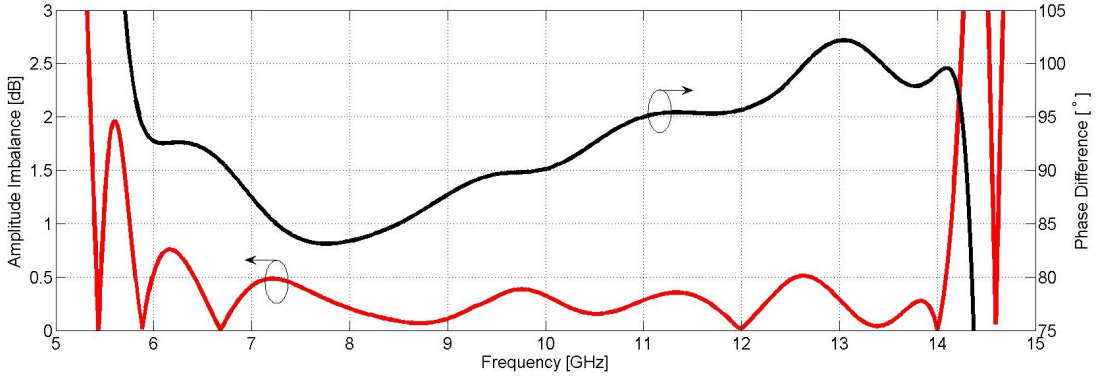

(b)

Figure 5.8: Results after EM simulation (2.5D) in ADS Momentum for the proposed design B with broadband matching networks. (a) S-parameters. (b) Amplitude imbalance and phase difference between the two output ports

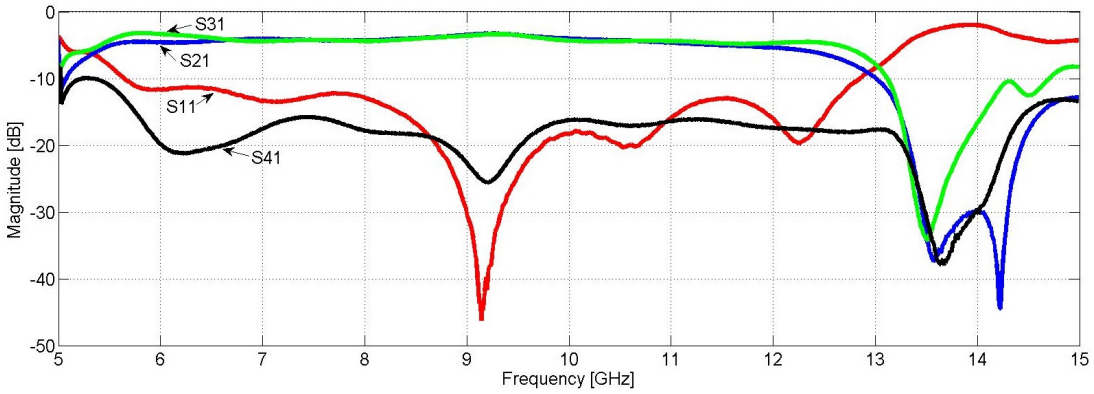

(a)

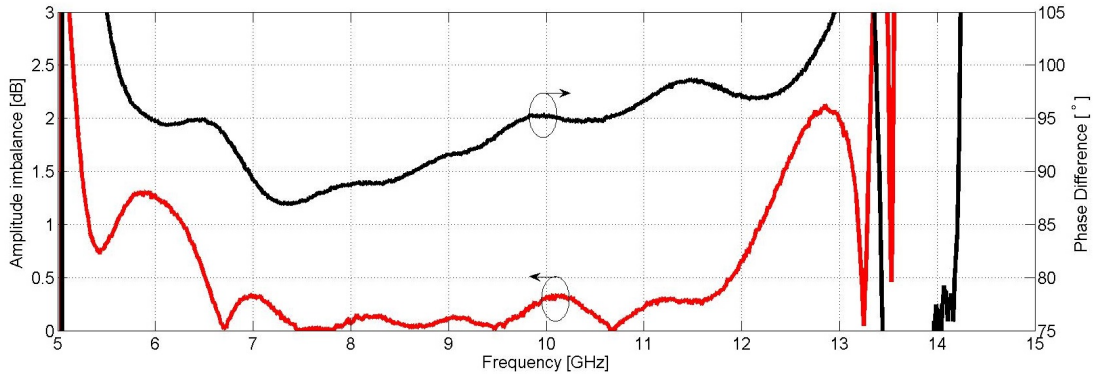

(b)

Figure 5.9: Measurement results for design B with broadband matching networks. (a) S-parameters. (b) Amplitude imbalance and phase difference between the two output ports

5.3 180 Degree Power Divider

This section contains the simulated and measured results for the 180° power divider presented earlier. The simulation and measurements are performed in the same way as the quadrature hybrids. Initially the results for the two separate devices will be presented: the Wilkinson power divider and the phase shifting network followed by the performance of the final device.

5.3.1 Wilkinson Power Divider

To begin with, the simulated and measured performance of the four stage Wilkinson power divider will be presented in figures 5.10 and 5.11 respectively. As one can see the measured and simulated results agree well with eachother. The measurements were only performed up to 16 GHz due to increased complexity in the calibration procedure, there was no need to explore higher frequencies for the final device due to bandwidth limitations in the phaseshifting network. A noticeable difference in phase imbalance can

be observed comparing the simulated and measured results and can be explained by solder-residue spreading unevenly between the two sides of the resistors.

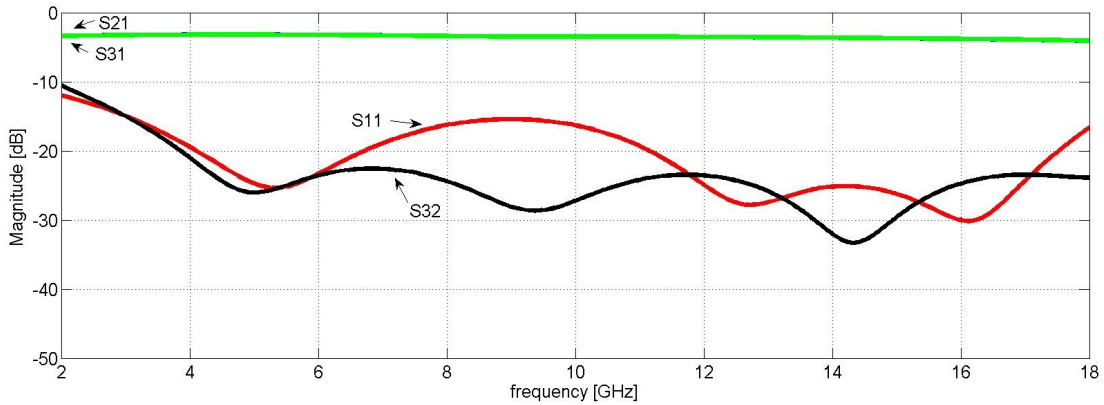

(a)

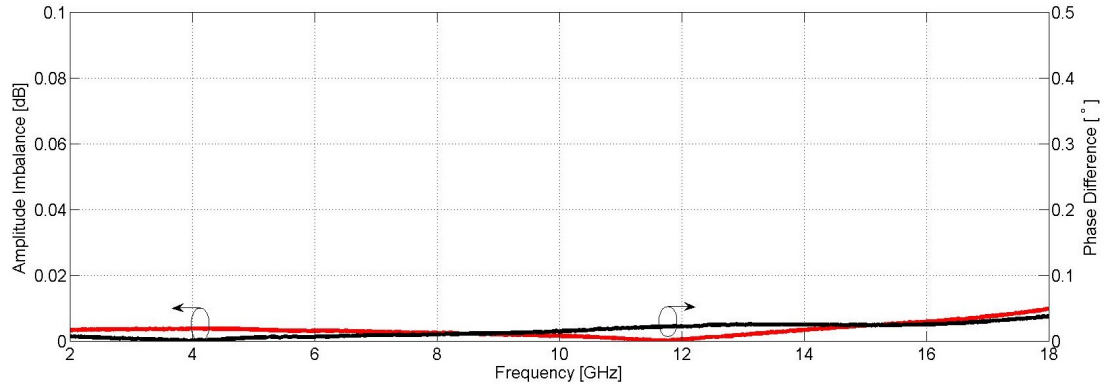

(b)

Figure 5.10: Results after EM simulation (2.5D) in ADS Momentum for the four-section Wilkinson power divider. (a) S-parameters. (b) Amplitude imbalance and phase difference between the two output ports, note the smaller scale on the y-axis

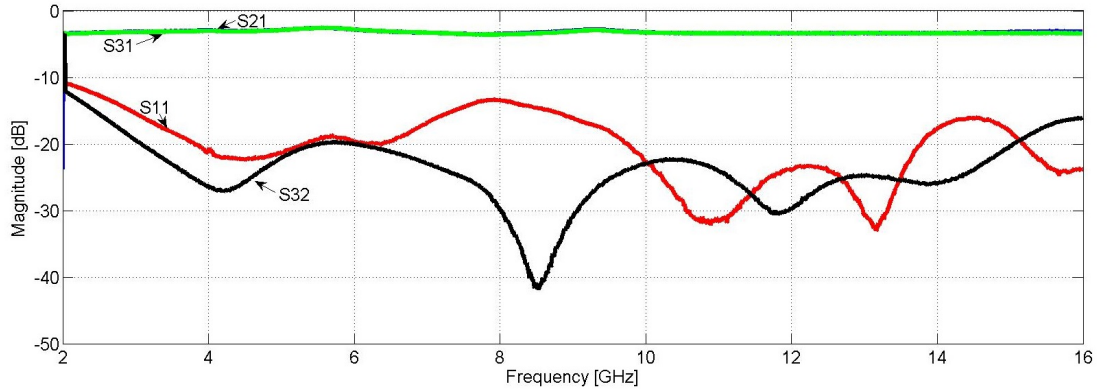

(a)

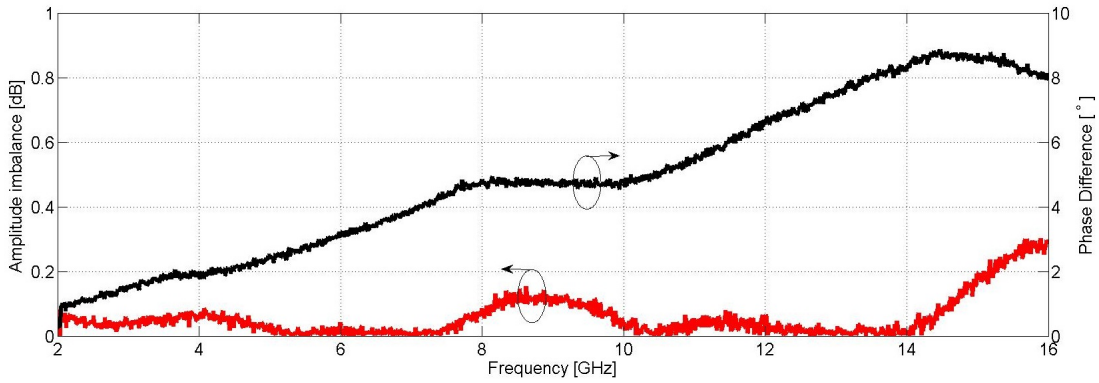

(b)

Figure 5.11: Measurement results for the four-section Wilkinson power divider. (a) S-parameters. (b) Amplitude imbalance and phase difference between the two output ports, note the smaller scale on the y-axes

5.3.2 Phaseshifter

The performance of the phaseshifting network is presented in figures 5.12 and 5.13. Figure 5.12 presents the EM-simulation performance and the results from the measurements are presented in figure 5.13. Except for a shift to a lower center frequency the simulated and measured results agree rather well. The frequency shift is probably caused by the same reasons stated earlier referring to the removal of the solder mask.

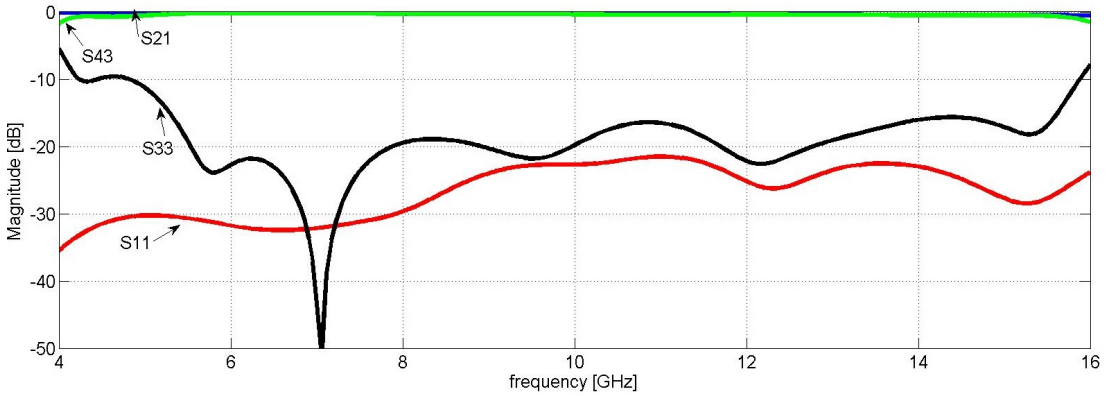

(a)

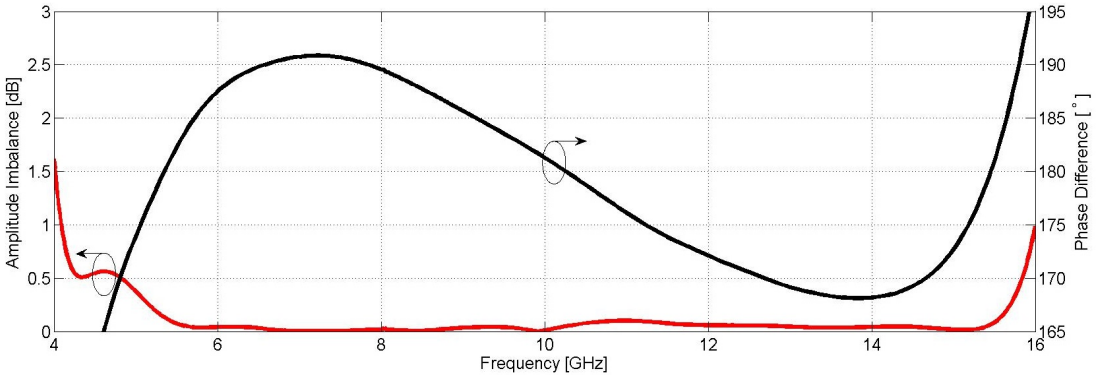

(b)

Figure 5.12: Results after EM simulation (2.5D) in ADS Momentum for the phaseshifting t-network. (a) S-parameters. (b) Amplitude imbalance and phase difference between the two output ports.

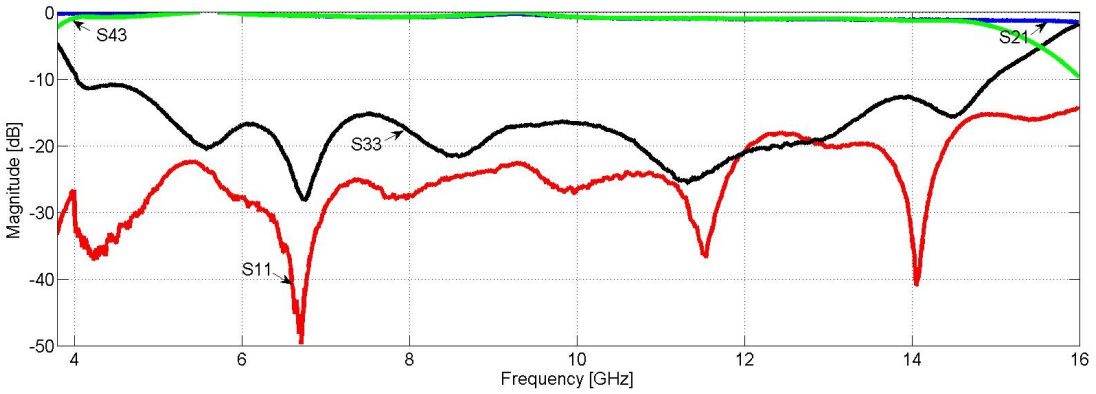

(a)

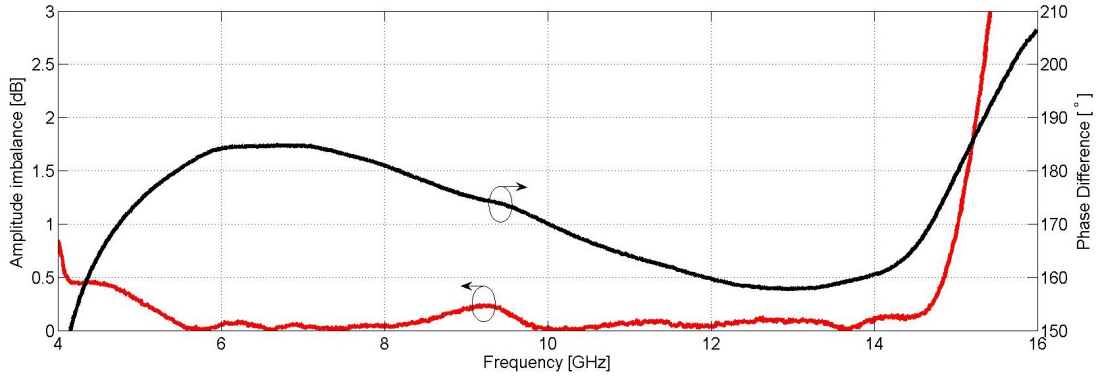

(b)

Figure 5.13: Measured performance of the phaseshifting t-network. (a) S-parameters. (b) Amplitude imbalance and phase difference between the two output ports.

5.3.3 180 Degree Power Splitter

Finally the performance of the final device, the 180° power splitter, is presented. The simulated and measured results are illustrated in figures 5.14 and 5.15 respectively.Just as for the phase shifting section the simulated and measured results agree very well except for the lowering of center frequency.

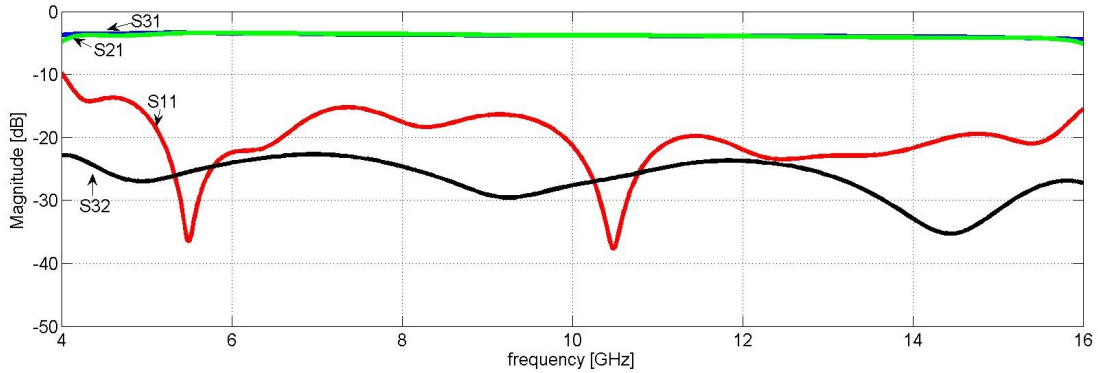

(a)

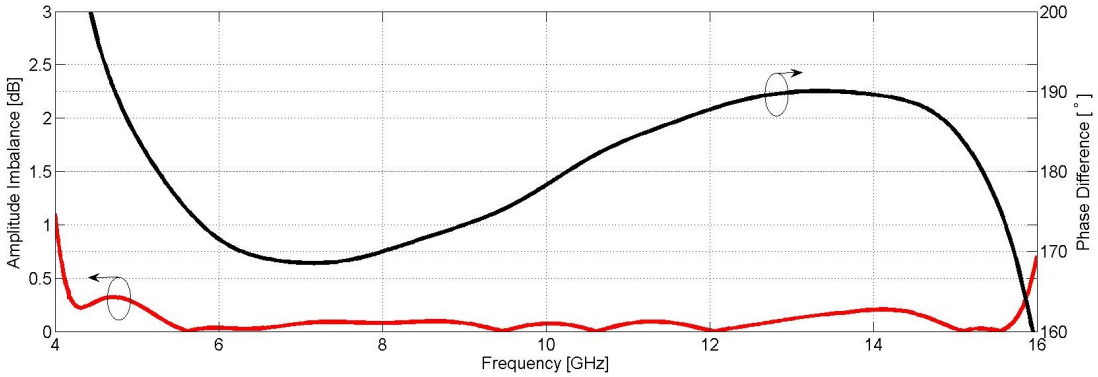

(b)

Figure 5.14: Results after EM simulation (2.5D) in ADS Momentum for the final 180 degree power splitter. (a) S-parameters. (b) Amplitude imbalance and phase difference between the two output ports

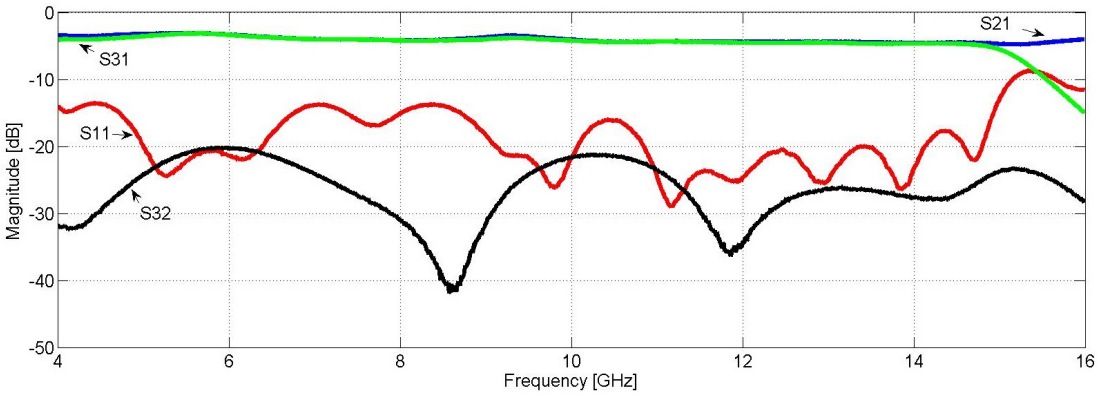

(a)

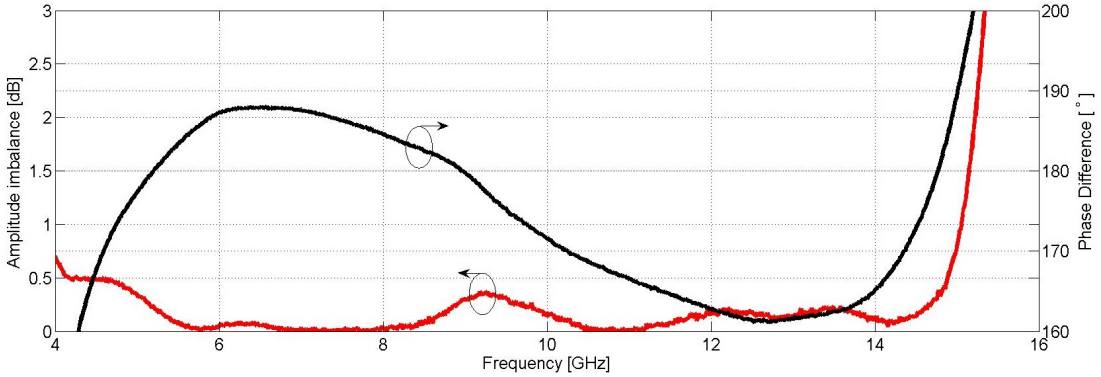

(b)

Figure 5.15: Measurement results for the final 180 degree power splitter. (a) S-parameters. (b) Amplitude imbalance and phase difference between the two output ports

5.4 Summary

A summary of the results, in terms some specification parameters, for the quadrature hybrids and 180 degree power splitter is presented in table 5.1 below. A recurring phase shift of 0.4 GHz - 0.7 GHz depending on device is detected and it probably originates from a combination of fabrication tolerances, rough scraping of the solder mask together with some oversight in the simulation parameters. The phase shift is in no way a severe problem for the thesis work since the bandwidth is the main parameter of interest and not a specific frequency band. Photographs of all the devices after the green solder mask had been scraped off the transmission lines are shown in figure 5.16.

Table 5.1: Table presenting the resulting key parameters from simulations and measurements for the quadrature hybrids and 180° power splitter

Device	**Center Frequency** (f_c)	**Fractional Bandwidth** ($\frac{\Delta f}{f_c}$)	**Size** [$mm \times mm$]	**Phase Difference**	**Amplitude Imbalance**
Design A *simulated*	9.88 GHz	38.4 %	6.5×9.1	$91.4° \pm 1.2°$	0.5 dB
Design A *measured*	9.42 GHz	32.1 %	6.5×9.1	$93.1° \pm 3.3°$	0.66 dB
Design A + stubs *simulated*	9.79 GHz	62.2%	25.4×29.9	$92.1° \pm 6.4°$	0.56 dB
Design A + stubs *measured*	9.32 GHz	42.0 %	25.4×29.9	$93.6° \pm 4.6°$	0.6 dB
Design B *simulated*	10.05 GHz	67.6 %	16.9×37.0	$91.7° \pm 7.3°$	0.5 dB
Design B *measured*	9.47 GHz	64.7 %	16.9×37.0	$94.8° \pm 8.8°$	1.26 dB
Design B + stubs *simulated*	9.95 GHz	83.6 %	26.3×56.3	$92.66° \pm 9.5°$	0.76 dB
Design B + stubs *measured*	9.25 GHz	59.5 %	26.3×56.3	$92.8° \pm 5.8°$	0.5 dB
180° power splitter *simulated*	10.24 GHz	107.7 %	27.4×29.1	$179.3° \pm 10.8°$	0.32 dB
180° power splitter *measured*	9.60 GHz	110.4 %	27.4×29.1	$174.5° \pm 13.4°$	0.5 dB

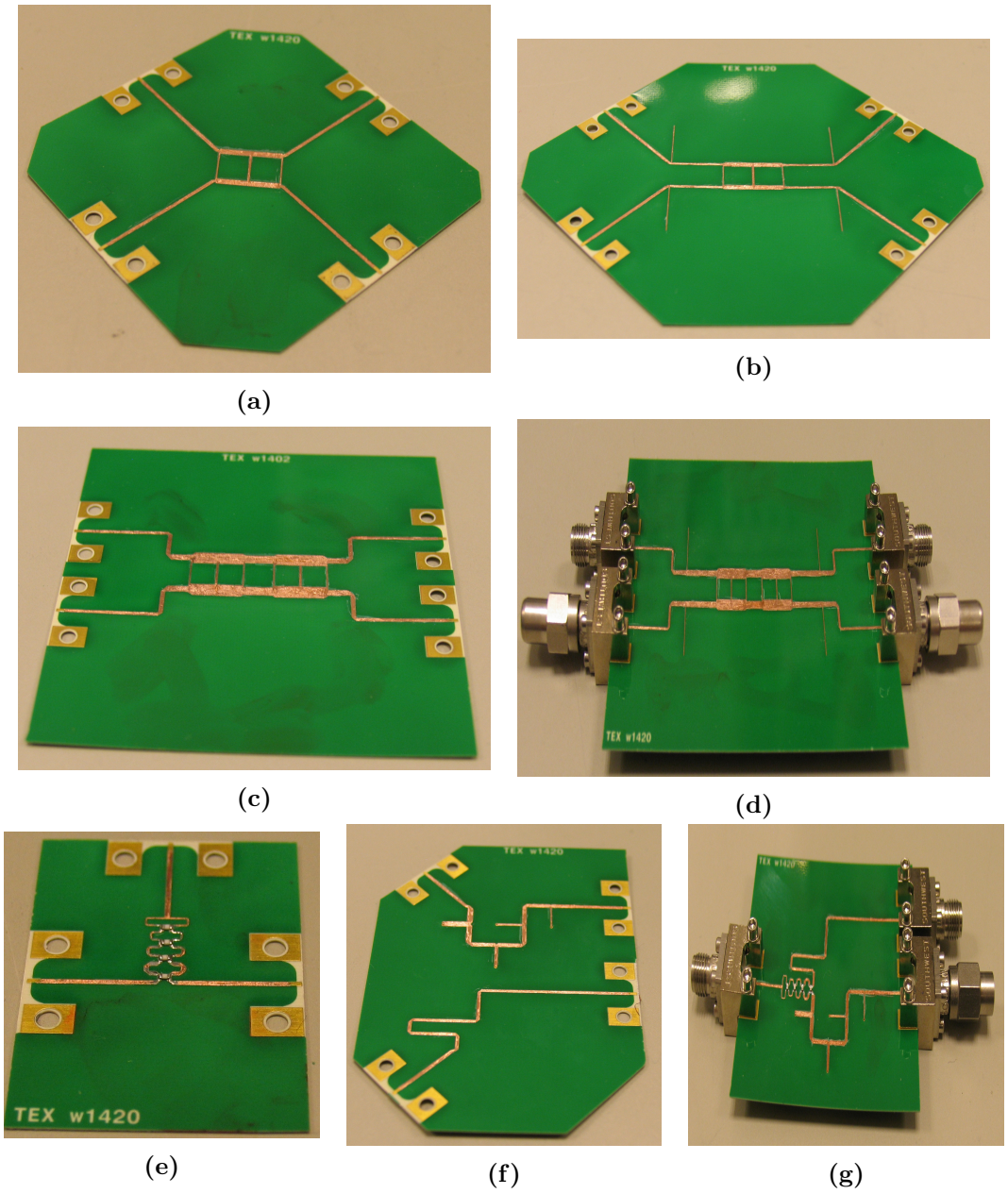

Figure 5.16: Photos of the manufactured devices after the solder-mask layer had been scarped off. (a) Design A. (b) Design A with broadband matching network. (c) Design B (d) Design B with broadband matching network, the chosen connectors described in chapter 5 can be seen here, two of the ports are terminated with 50Ω loads (e) 4-section Wilkinson power divider (f) Phase shifting network (g) 180° power splitter with connectors and a termination on one of the output ports.

5.5 Comparison

A comparison between the quadrature hybrid proposed in this thesis (Design B with Broadband matching network) and other quadrature hybrids presented in scientific literature is done in table 5.2. The proposed design performs well in comparison with other designs despite the complications in fabrication. A similar comparison is made for the out-of-phase power splitter in table 5.3 and it can yet again be concluded that the proposed design compares very well with the other proposed designs.

Table 5.2: Comparison between the novel design quadrature hybrid of this work and other relevant quadrature hybrids.

Device	**Transmission Line**	f_c **[GHz]**	**Fractional Bandwidth** ($\frac{\Delta f}{f_c}$)	**Size [mm × mm]**	**Phase Difference**	**Amplitude Imbalance**
Design B + stubs	*Microstrip*	*9.25*	*59.5 %*	26.3 × 56.3	92.8° ± 5.8°	*0.5 dB*
[3]	Microstrip	2	56 %	29 × 37	90° ± 3°	≈1.3 dB
[27]	Microstrip	2	45 %	24.4 × 35.5	No Data	≈ 3 dB
[28]	PolyStrata	29	76 %	8.2 × 25.9	90° ± 15°	1.6 dB
[29]	Stripline	5.5	164 %	44 × 120 × 13	90° ± 7°	1.5 dB
[30]	Microstrip	4	75 %	No Data	90° ± 5°	≈5.0 dB

Table 5.3: Comparison between the 180° power splitter of this thesis and other relevant work.

Device	**Transmission Line**	f_c **[GHz]**	**Fractional Bandwidth** ($\frac{\Delta f}{f_c}$)	**Size [mm × mm]**	**Phase Difference**	**Amplitude Imbalance**
This work	*Microstrip*	*9.6*	*110 %*	27.4 × 29.1	174.5° ± 13.4°	*0.5 dB*
[31]	Microstrip	2.8	67 %	57 × 100	180° ± 10°	0.5 dB
[32]	Microstrip - Slotline	7	115 %	20 × 40	180° ± 0.25°	≈0.4 dB
[33]	Microstrip	6	66 %	6 × 6	180° ± 9°	≈2 dB

6

Conclusion

Four different quadrature hybrids and one out-of-phase power splitter have been designed and verified by measurements in this thesis. The quadrature hybrid simulations and measurements did not agree completely with each other and reasons behind this could come from the manufacturing complication. It is difficult to estimate how much the devices were affected by this and how much fabrication inaccuracies are to blame, but it is leaning towards fabrication inaccuracies. This is because the 180° splitter was hardly affected even though it went through the same scraping-treatment, also the quadrature hybrids proved to be sensitive to changes in impedance of the transmission lines while the out-of-phase power splitter is more robust in that sense.

Despite this, remembering that the objective was not to produce a finished product but more so to present concepts regarding wideband operation and easy manufacturing as focal points, both of which were achieved. The proposed quadrature hybrid, named *Design B* here, shows great promise and compares well with other competing designs as can be seen in table 5.2. For applications that do not put immense importance on size, the proposed quadrature hybrid can very well be an attractive option especially due to the fact that it is entirely fabricated using microstrip technology. The broadband matching technique proved to work rather well and had a stabilising effect seen to the amplitude imbalance when comparing with the devices without. In conclusion a novel quadrature hybrid was designed with an amplitude imbalance and phase imbalance of less than 0.5 dB and 6° respectively, isolation and return loss were better than 10 dB over a fractional bandwidth of 59.5%, a bandwidth that probably can reach the simulated levels of above 80% if manufacturing mistakes are avoided.

As mentioned the thesis also presents the design and verification by measurements of a 180° power splitter fabricated using entirely planar microstrip technology. The power divider is made up out of a wideband multi-section Wilkinson power divider together with a phase shifting network. The phase shift comes from the phase difference between

a phase shifting t-network section and a transmission line. The device has a measured fractional bandwidth of 110 % with a return loss and isolation better than 13.5 dB and 20 dB respectively. Amplitude and phase imbalance are better than 0.5 dB and 13.4° respectively. The design shows great performance in comparison with other designs, see table 5.3 and it can easily be designed to give a quadrature split by removing a $\lambda_c/4$ piece from the delay-line at one of the output ports. The device also shows great robustness and the performance was not noticeably affected by the solder mask scraping in contrast to the quadrature hybrids. To the authors knowledge the proposed device has the widest fractional bandwidth for a 180° power divider assuming a better than 20 dB isolation.[1]

[1]The same claim was made in [33] with better than 15 dB isolation and a fractional bandwidth of 66 %.

A

Appendix A

This appendix aims to present an analysis of the phase shifting T-network described in the paper. To keep the size of the expressions in the matrices at a comprehending level a single section, see figure A.1, will be analysed initially and a more general expression will be derived at the end. One section of the network consists of a grounded shunt ($90° = \frac{\lambda}{4}$ at center frequency) transmission line with impedance Z_1 and two series 90° transmission lines with impedance Z_2 and Z_3. The shunt and series lines control the phase response and return loss respectively. The shunt line has an insertion phase of 0° and the series lines have an insertion phase of 180°. As described in the paper, by attachment of a 360° transmission line to the second output port of a power divider and by careful selection of Z_1, a broadband constant 180° phase shift can be achieved.

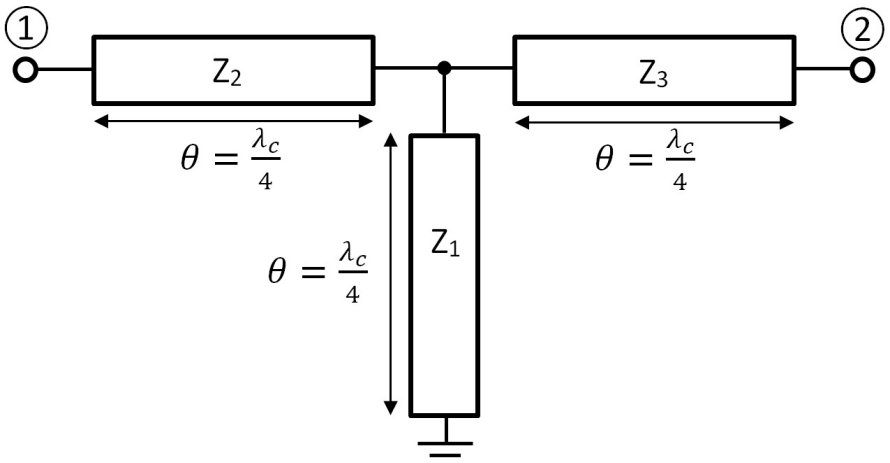

Figure A.1: A single section of the phase shifting T-network.

Starting off by expressing the ABCD-matrix for the single section T-network:

$$\begin{bmatrix} A & B \\ C & D \end{bmatrix} = \begin{bmatrix} \cos(\theta) & jZ_2\sin(\theta) \\ \frac{j}{Z_2}\sin(\theta) & \cos(\theta) \end{bmatrix} \begin{bmatrix} 1 & 0 \\ \frac{-j}{Z_1}\cot(\theta) & 1 \end{bmatrix} \begin{bmatrix} \cos(\theta) & jZ_3\sin(\theta) \\ \frac{j}{Z_3}\sin(\theta) & \cos(\theta) \end{bmatrix}$$
$$= \begin{bmatrix} (1+\frac{Z_2}{Z_1})\cos^2(\theta) - \frac{Z_2}{Z_3}\sin^2(\theta) & j(Z_3 + \frac{Z_2Z_3}{Z_1} + Z_2)\cos(\theta)\sin(\theta) \\ j[(\frac{1}{Z_2}+\frac{1}{Z_3})\cos(\theta)\sin(\theta) - \frac{1\cos^3(\theta)}{Z_1\sin(\theta)}] & (1+\frac{Z_3}{Z_1})\cos^2(\theta) - \frac{Z_3}{Z_2}sin^2(\theta) \end{bmatrix} \tag{A.1}$$

Assume that the impedances of the transmission lines at both sides of the shorted stub are equal ($Z_2 = Z_3$), Z_2 will be used to express that impedance. The resulting elements of the ABCD-matrix:

$$\begin{aligned} A &= \cos^2(\theta) - \sin^2(\theta) + \frac{Z_2}{Z_1}\cos^2(\theta) \\ B &= jZ_2(2+\frac{Z_2}{Z_1})\cos(\theta)\sin(\theta) \\ C &= j(\frac{2}{Z_2}\cos(\theta)\sin(\theta) - \frac{1}{Z_1}\cot(\theta)\cos^2(\theta)) \\ D &= \cos^2(\theta) - \sin^2(\theta) + \frac{Z_2}{Z_1}\cos^2(\theta) \end{aligned} \tag{A.2}$$

It is clear that we area dealing with a symmetrical device since $A = D$, now to derive an expression for the reflection coefficient Γ (Normalised to $Z_0 = 50\Omega$):

$$\begin{aligned} \Gamma = S_{11} &= \frac{A+B-(C+D)}{A+B+C+D} = \frac{B-C}{A+B+C+D} \\ &= j[Z_2(2+\frac{Z_2}{Z_1})\cos(\theta)\sin(\theta) + \frac{1}{Z_1}\cot(\theta)\cos^2(\theta) - \frac{2}{Z_2}\cos(\theta)\sin(\theta)] \\ &= j\sin^2(\theta)\cot(\theta)[(2Z_2 + \frac{Z_2^2}{Z_1} - \frac{2}{Z_2}) + \frac{1}{Z_1}\cot^2(\theta)] \end{aligned} \tag{A.3}$$

This equation has to be solved numerically, it can be done with help functions like in the synthesis for multi-section branch line couplers in the papers by Levy & Lind and Muraguchi et al. Here it can be chosen if maximally flat characteristics (Butterworth) or equal ripple characteristics (Chebychev) are wanted. As an example, equal ripple characteristics were chosen, and by tuning in the simulation software these values for the impedances emerged: $Z_1 = 18\Omega$ and $Z_2 = 31\Omega$. Those values give three reflection zeros, one at the center frequency (f_c) and two equally spaced around f_c. The maximal VSWR was chosen to be 1.20 and with $f_c = 12$ GHz the bottom and top frequencies

were 7.4 GHz and 16.6 GHz respectively, resulting in a 77 % bandwidth for the single section T-network.

And to generalise the concept, for a T-network with m number of sections the resulting ABCD-matrix can be computed with:

$$\begin{bmatrix} A & B \\ C & D \end{bmatrix} = \frac{j^{(2m)}}{(1-W^2)^m} \prod_{i=1}^{m} \begin{bmatrix} 1+W^2(1+\frac{Z_{2i}}{Z_{1i}}) & Z_{2i}W(2+\frac{Z_{2i}}{Z_{1i}}) \\ W\frac{2}{Z_{2i}} + \frac{W^3}{Z_{1i}} & 1+W^2(1+\frac{Z_{2i}}{Z_{1i}}) \end{bmatrix} \tag{A.4}$$

Where $W = -j\cot(\theta)$ and Z_{1i}, Z_{2i} are the impedances for the $\frac{\lambda}{4}$ shorted stub and the $\frac{\lambda}{4}$ transmission lines on the i :th section.

Bibliography

[1] D. M. Pozar, Microwave Engineering, 4th Edition, John Wiley and Sons Inc, 2012.

[2] C. Potter, G. Hjipieris, Improvements in ultra-broadband tem coupler design, IEE Proceedings H Microwaves, Antennas and Propagation 139 (2) (1992) 171–178.

[3] Y.-H. Chun, J.-S. Hong, Compact wide-band branch-line hybrids, Microwave Theory and Techniques, IEEE Transactions 54 (2) (2006) 704–709.

[4] J. Reed, G. Wheeler, A method of analysis of symmetrical four-port networks, Microwave Theory and Techniques, IRE Transactions 4 (4) (1956) 246–252.

[5] R. Levy, L. Lind, Synthesis of symmetrical branch-guide directional couplers, Microwave Theory and Techniques, IEEE Transactions 16 (2) (1968) 80–89.

[6] M. Muraguchi, T. Yukitake, Y. Naito, Optimum design of 3-db branch-line couplers using microstrip lines, Microwave Theory and Techniques, IEEE Transactions 31 (8) (1983) 674–678.

[7] W. Marynowski, A. Kusiek, A. Walesieniuk, J. Mazur, Investigations of broadband multilayered coupled line couplers, in: 14th Microwave Techniques Conference, IEEE, Prague, Czech Republic, 2008, pp. 1–4.

[8] R. Mongia, I. B. P. Bhartia, J. Hong, RF and Microwave Coupled-Line Circuits, 2nd Edition, Artech House, 2007.

[9] R. Garg, I. Bahl, Characteristics of coupled microstriplines, Microwave Theory and Techniques, IEEE Transactions 27 (7) (1979) 700–705.

[10] L. Young, The analytical equivalence of tem-mode directional couplers and transmission-line stepped-impedance filters, Electrical Engineers, Proceedings of the Institution 110 (2) (1963) 275–281.

[11] O. Kizilbey, O. Palamutcuogullari, B. Yarman, A miniaturized wideband 180° hybrid ring coupler, in: 14th Annual Wireless and Microwave Technology Conference (WAMICON), IEEE, Orlando, FL, 2013, pp. 1–4.

[12] K. Chan, A. Tan, K. Rambabu, Design and analysis of a decade bandwidth 180° hybrid coupler, Electronics Letters, IET 7 (1) (2013) 71–77.

[13] S. B. Cohn, A class of broadband three-port tem-mode hybrids, IEEE MTT-16 (2) (1968) 110–118.

[14] G. P. Riblet, A directional coupler with very flat coupling, Microwave Theory and Techniques, IEEE Transactions 26 (2) (1978) 70–74.

[15] A. S. Wright, Very broadband flat coupling hybrid ring, Electronics letters 23 (1) (1987) 47–49.

[16] J. V. Ashforth, Design equations to realise a broadband hybrid ring or a two-branch guide coupler of any coupling coefficient, Electronics letters 24 (20) (1989) 1276–1277.

[17] B. Mayer, R. Knochel, Branchline-couplers with improved design flexibility and broad bandwidth, in: Microwave Symposium Digest, 1999 IEEE MTT-S International, IEEE, Dallas, TX, USA, 1990, pp. 391–394.

[18] E. Johansson, Mönsterkort, från CAD till kort, 2nd Edition, Sveriges Verkstadsindustrier, Industrilitteratur AB, 2002.

[19] H. Rashid, D. Meledin, V. Desmaris, V. Belitsky, Novel waveguide 3 db hybrid with improved amplitude imbalance, Microwave and Wireless Components Letters, IEEE 24 (4) (2014) 212–214.

[20] R. Knochel, Broadband flat coupling two-branch and multibranch directional coupler, in: Microwave Symposium Digest, 1999 IEEE MTT-S International, IEEE, Anaheim, CA, USA, 1999, pp. 1327–1330.

[21] X. Tang, K. Mouthaan, Ultra-wideband quadrature power splitter, Microwave and Optical Technology Letters 52 (12) (2010) 2828–2830.

[22] E. J. Wilkinson, An n-way hybrid power divider, IEEE 8 (1) (1960) 116–118.

[23] M. Caillet, M. Clenet, A. Sharaiha, Y. Antar, A compact wide-band rat-race hybrid using microstrip lines, Microwave and Wireless Components Letters, IEEE 19 (4) (2009) 191–193.

[24] W. Chang, C. Liang, C. Chang, Wideband high-isolation and perfect-balance microstrip rat-race coupler, Electronics Letters, IET 48 (7) (2012) 382–384.

[25] W.L. Gore and Associates, `http://www.gore.com/MungoBlobs/47/733/Gore_Phaseflex_10_18_13_app.pdf`, GORE PHASEFLEX Microwave/RF test assemblies.

[26] Southwest Microwave, `http://mpd.southwestmicrowave.com/showImage.php?image=832&name=End_Launch_Connectors.pdf`, End Launch Connecto Series.

[27] B. Alqahtani, A. Sheta, M. Alkanhal, New compact wide-band branch-line couplers, in: 39th European Microwave Conference, European Microwave Association (EuMA), Rome, Italy, 2009, pp. 1–4.

[28] N. Sutton, J. Oliver, D. Filipovic, Wideband 18–40 ghz surface micromachined branchline quadrature hybrid, Microwave and Wireless Components Letters, IEEE 22 (9) (2012) 462–463.

[29] S. Javadzadeh, S. Majedi, F. Farzaneh, An ultra-wideband 3-db quadrature hybrid with multisection broadside stripline tandem structure, in: 6th International ICST Conference, MOBIMEDIA 2010, Lisbon, Portugal, 2010, pp. 672–681.

[30] J. Bonney, J. Schoebel, Synthesis of extremely flat broadband multi-section quadrature coupler, in: Microwave Conference (GeMIC), 2008 Germany, German Institute for Microwave and Antenna Technologies (IMA), Hamburg-Harburg, Germany, 2008, pp. 1–4.

[31] M. Basraoui, S. Prasad, Wideband, planar, log-periodic balun, in: Microwave Symposium Digest, 1998 IEEE MTT-S International (2), MOBIMEDIA 2010, Baltimore, MD, USA, 1998, pp. 785–788.

[32] M. Bialkowski, A. Abbosh, Design of a compact uwb out-of-phase power divider, Microwave and Wireless Components Letters, IEEE 17 (4) (2007) 289–291.

[33] A. Abbosh, Planar out-of-phase power divider/combiner for wideband high power microwave applications, Components, Packaging and Manufacturing Technology, IEEE Transactions on 4 (3) (2013) 465–471.